REPORT DOCUMENTATION PAGE

Form Approved
OMB No. 0704-0188

Public reporting burden for this collection of information is estimated to average 1 hour per response, including the time for reviewing instructions, searching existing data sources, gathering and maintaining the data needed, and completing and reviewing this collection of information. Send comments regarding this burden estimate or any other aspect of this collection of information, including suggestions for reducing this burden to Department of Defense, Washington Headquarters Services, Directorate for Information Operations and Reports (0704-0188), 1215 Jefferson Davis Highway, Suite 1204, Arlington, VA 22202-4302. Respondents should be aware that notwithstanding any other provision of law, no person shall be subject to any penalty for failing to comply with a collection of information if it does not display a currently valid OMB control number.
PLEASE DO NOT RETURN YOUR FORM TO THE ABOVE ADDRESS.

1. REPORT DATE *(DD-MM-YYYY)*	2. REPORT TYPE	3. DATES COVERED *(From - To)*
10-05-2007		Nov. 2003 – Nov. 2006

4. TITLE AND SUBTITLE
Turbulence and Complex Flow Phenomena in Axial Turbomachines

5a. CONTRACT NUMBER

5b. GRANT NUMBER
FA9550-04-1-0019

5c. PROGRAM ELEMENT NUMBER

6. AUTHOR(S)

Katz, Joseph and Meneveau, Charles

5d. PROJECT NUMBER

5e. TASK NUMBER

5f. WORK UNIT NUMBER

7. PERFORMING ORGANIZATION NAME(S) AND ADDRESS(ES)

The Johns Hopkins University
Department of Mechanical
Engineering
3400 N. Charles St.
Baltimore, MD 21218

8. PERFORMING ORGANIZATION REPORT NUMBER

9. SPONSORING / MONITORING AGENCY NAME(S) AND ADDRESS(ES)
Air Force Office of
Scientific Research
801 North Randolph Street
Arlington VA, 22203-1977
Dr Rhett Jeffries / NA

10. SPONSOR/MONITOR'S ACRONYM(S)
AFOSR/NA

11. SPONSOR/MONITOR'S REPORT NUMBER(S)

12. DISTRIBUTION / AVAILABILITY STATEMENT

Approved for public release,
distribution unlimited

AFRL-SR-AR-TR-07-0170

13. SUPPLEMENTARY NOTES

14. ABSTRACT

The objective of this project is to measure the flow within axial turbomachines and use the data to address turbulence modeling issues. Measurements are performed in two-stage transparent machines located in an optically index matched facility, which allows unobstructed 2-D and Stereo PIV measurements. Data provide insight on blade–wake, wake-boundary layer and wake–wake interactions. This report examines and elucidates several phenomena: i. Variations in turbulence within a wake generated by an upstream IGV blade while being ingested by a rotor passage; ii. Non-uniform turbulence production and diffusion leading to formation of turbulent hot spots within a rotor wake due to flow non-uniformities generated by upstream wakes; iii. Unsteady flow caused by an upstream wake stabilizes the boundary layer on a rotor blade and reduces its momentum thickness; iv. Comparisons of data covering an entire stage to RANS predictions; and v. Measurements of subgrid-scale stresses and dissipation rate, and comparisons to model predictions as well as associated implications of spatial averaging followed by ensemble averaging in spatially non-uniform flows.

15. SUBJECT TERMS
Particle Image Velocimetry, turbomachines, Turbulence, wake-wake interactions, wake-blade interactions, Reynolds stresses, Subgrid Stresses

16. SECURITY CLASSIFICATION OF:			17. LIMITATION OF ABSTRACT	18. NUMBER OF PAGES	19a. NAME OF RESPONSIBLE PERSON
a. REPORT	b. ABSTRACT	c. THIS PAGE			19b. TELEPHONE NUMBER *(include area code)* 410-516-5470

Final Report

TURBULENCE AND COMPLEX FLOW PHENOMENA IN MULTI-STAGE AXIAL TURBOMACHINES

AFOSR GRANT # FA9550-04-1-0019

Submitted by

Joseph Katz & Charles Meneveau

Department of Mechanical Engineering
The Johns Hopkins University
Baltimore, MD 21218

This project was sponsored by the Air Force Office of Scientific Research under grant No. FA9550-04-1-0019. The program managers have been T. Beutner and R. Jeffries

1.0 Executive Summary

This report summarizes our effort to measure unsteady flows in turbomachines, and use the data for addressing relevant turbulence-modeling issues. The experiments are being performed in a two-stage, axial-turbomachine, flow visualization facility containing fluid (solution of NaI in water) with an optical index of refraction that matches that of the acrylic blades. The unobstructed view on an entire stage enable measurements of two and three velocity components in numerous sample planes using 2D and stereo PIV (Particle Image Velocimetry). Data provide insight into the flow within turbomachines at unprecedented levels of detail, enabling us to investigate various wake-blade, wake-wake and wake-boundary layer interactions. Turbulence and unsteady flow phenomena are being examined at three levels: (i) Passage-averaged, steady RANS; (ii) Unsteady RANS, and (iii) Large-Eddy-Simulation (LES).

In the context of unsteady RANS, we examine the turbulence within a wake generated by an upstream IGV blade as it impinges on a rotor blade and is ingested by a rotor passage. Several phenomena involving the non-uniform strain field encountered by the wake, some causing negative production rate, substantially alter the distributions of Reynolds stresses. Furthermore, data obtained in multiple, closely spaced planes show that non-uniform turbulence production and diffusion caused by wake shearing explains the non-uniform distribution of Reynolds stresses, and cause formation of turbulent hot spots. Another study shows that unsteady flow caused by impingement of an upstream wake on a rotor blade stabilizes the boundary layer and reduces its momentum thickness. Comparisons of data covering an entire stage to RANS predictions of the same flow using several standard Reynolds stress models show major discrepancies. These are traced to difficulties in predicting pressure-strain correlation terms.

In the context of LES, spatial filtering of the data enables direct measurements of subgrid-scale (SGS) stresses, SGS dissipation rate, and comparisons to model predictions. Utilizing rotor wake data, we examine the implications of spatial averaging followed by ensemble averaging in spatially non-uniform flows. The analysis has helped explain observed differences between turbulent kinetic energy production (RANS) and SGS dissipation rates (LES), important issues that arise at the RANS-LES interface.

The experimental and analysis obtained to-date have already been presented in journal papers, eight of which are already published and one is still under review. In addition, twenty conference papers have been presented in IGTI, AIAA and ASME-FED conferences. A complete list of publications is provided in Section 5. For the Soranna et al. (2005b) paper, we received the *Knapp Award* for the best paper presented in the ASME, Fluids Engineering Division Summer Meeting, 2005, with analytical, numerical and laboratory research.

Construction of the turbomachinery facility and the research performed in it has been funded in part by AFOSR and in part by ONR. Each has also provided support for one graduate student and 50% of the post doc salary during the period covered under this grant. One of the Post Docs, O. Uzol, is presently an Assistant Prof. at the Middle East Technical University in Turkey. One of the graduate students, Y.C. Chow, completed his graduate studies and received a PhD degree. He is currently employed as an Assistant Prof. in National Taiwan Ocean University.

4. Objectives and Rationale for this Research Program

In this study, we examine turbulence and unsteady flow phenomena within complex turbomachinery flow. The data are interrogated from the viewpoint of three distinct modeling levels: (i) Passage-averaged, steady RANS, (ii) Unsteady RANS, and (iii) Large-Eddy-Simulation (LES).

The "average-passage" RANS equations, introduced by Adamczyk (1985) compute time-averaged flows within multi-stage turbomachines, while using steady boundary conditions, but still accounting for blade-rows interactions. This approach is an essential practical design tool for turbomachines with multiple blade rows and varying number of rotor and stator blades in consecutive stages. In this method, each blade row has a steady average-passage flow field extending over the entire machine. Neighboring blade rows are replaced with circumferentially uniform systems of body forces, energy sources and deterministic stresses (Adamczyk, 1986; Adamczyk et al., 1986, 1990; Rhie et al., 1998; LeJambre et al., 1998; Busby et al., 2000). Effects of phase-dependent unsteadiness on the average-passage flow field are accounted for through the deterministic stresses, which must be modeled (e.g. Adamczyk, 1986; Van de Wall 2000; Meneveau & Katz, 2002; He et al., 2002). Unlike RANS closure models, there are no widely accepted and validated models whose development requires a database obtained either from experiments or from unsteady RANS simulations of multiple stages. In previous experimental studies, the deterministic stresses have been obtained either by traversing single point sensors (e.g. Prato et al., 1997, 1998; Suryavamshi et al., 1998a, b), or by Particle Image Velocimetry (PIV) measurements (Sinha et al., 2000; Uzol et al., 2002b, 2003a, 2004b), some in our optically refractive index matched facility.

At a level more detailed than average-passage RANS, modeling turbulent flows using Unsteady RANS continues to be a primary computational tool for prediction of turbomachinery flows. While LES has been displacing Unsteady RANS in some simple geometry applications, it is undisputed that RANS will continue to play an important role in simulation of relevant flows. Its role has been recently enhanced in applications in which RANS is applied together with LES in hybrid approaches (Piomelli & Balaras, 2002). RANS is used to provide "outer, or inlet, boundary conditions" to LES performed in sub-regions of the flow, or to provide near-wall modeling, where LES may not be able to resolve viscous sublayers while RANS models based on 2D boundary-layer approximations allows wall-normal resolutions not affordable in LES.

Applications of Unsteady RANS simulations have introduced numerous uncertainties associated with Reynolds stress closure models. In spite of many decades of advancements, too many to summarize in a single proposal, there are still fundamental unresolved problems in applications of RANS particularly in highly strained, spatially non-uniform, non-equilibrium, unsteady flows that characterize turbomachines. Some of these issues are described in § 4.3 of this report using, as an example, an application of RANS to model turbomachinery flow. Other issues are discussed as we present data on the evolution of Reynolds stresses within a rotor passage in § 4.2. Testing, validation and development of Reynolds stress models requires data obtained in relevant flow conditions, a challenging task as far as turbomachines are concerned. Single-point data are inherently limited. Due to optical obstruction and reflection from boundaries, applications of global techniques in turbomachines, such as PIV, have been limited to parts of blade passages, e.g. away from boundary layers and from near wake of blades (e.g. Tisserant et al., 1997; Gogineni et al., 1997; Balzani et al., 2000; Wernet, 2000; Sanders et al., 2002). In facilities involving compressible flows, these problems seem to be unavoidable. However,

characterization of the interactions between blade-rows, e.g. wake-wake, wake-blade, wake-boundary layer interactions and impingement of trailing vortices on blades, require a complete picture on the mean flow structure and turbulence. Furthermore, the main turbulence modeling difficulties occur near boundaries, within boundary layers, in regions with high pressure-gradients such as the vicinity of a blade leading edge, and in very near wakes.

To address the challenging turbulence modeling issues, we have constructed a facility that enables unobstructed optical access using transparent rotor and stator blades operating in a liquid, which has the same optical index of refraction as the blades. Details on this facility along with several optical setups are provided §3. Subsequently, as demonstrated in §4, the measured flow structure and turbulence parameters provide unobstructed and unparalleled insights on dominant phenomena and their causes within the complex system of interacting turbulent wakes and blades.

The lingering issues with applications of RANS have contributed to the increasing popularity of Large Eddy Simulations (LES). In LES, we solve for the large-scale (resolved) turbulent motions using the spatially filtered Navier Stokes Equations. This filtering process introduces the sub grid scale (SGS) stress tensor that must be modeled in terms of resolved flow parameters, a process that has introduced its own series of issues (Leonard, 1974; Piomelli et al., 1991; Meneveau & Katz, 2000), especially near boundaries (Piomelli & Balaras, 2002). A key parameter in typical SGS stress modeling is the so-called SGS dissipation, which represents the flux of energy from resolved to sub-grid scales, and appears with opposite signs in the evolution equations of resolved and SGS kinetic energy. Since PIV provides instantaneous spatial distributions of velocity it can be filtered at different scales, making it an ideal tool for measuring the SGS stresses and dissipation, as well as for evaluating predictions of various models (Liu et al. 1994, 1999, Chen et al., 2005a, 2006, Sinha et al., 2000a, b, Chow et al. 2005a). In §4.6 we use the data to address issues brought about by spatial filtering followed by ensemble averaging of a spatially non-uniform flow. Such issues are of fundamental significance in merging LES and RANS which is expected to play a significant role for turbomachinery flow simulations. This analysis clarifies fundamental differences between SGS dissipation and turbulence production rate.

Construction of the turbomachinery facility (and two different sets of blade rows), and the research performed in it has been funded in part by AFOSR and in part by ONR. Each has provided support for one graduate student and 50% of the post doc salary. The AFOSR project has focused on blade-rows interactions and associated turbulence, and the ONR sponsored activity has dealt with stability of swirling flows, and issues in hydroacoustics of turbomachines. Inherently some of the topics to-date overlap.

3. Facilities and Techniques

3.1 Refractive Index Matched Facility and Blades

The axial turbomachine test facility, shown schematically in Figure 3.1a enables us to perform PIV measurements at any point within an entire (second) stage including the rotor, stator, gap between them, inflow into the rotor and the wake downstream of the stator. The unobstructed optical access is facilitated using a rotor and stator made of a transparent material (acrylic) that has the same optical index of refraction as the working fluid, a concentrated solution, 62%- 64% by weight, of NaI in water. This fluid has a specific gravity of 1.8 and a kinematic viscosity of 1.1×10^{-6} m^2/s, i.e. very close to that of water. Thus, the blades become almost invisible, do not obstruct the field of view, do not alter the direction of the illuminating laser sheet while passing through the blades, and minimize the reflection from boundaries. We have chosen this liquid over organic fluids due to its low viscosity, non-toxicity, ability to adjust the refractive index by adding salt, and relative ease of maintenance. Information related to use and maintenance of the NaI solution can be found in Uzol et al. (2002a). NaI is expensive but there is no need to provide means to prevent algae growth, and there is no need to replace the water due to the high salt concentration. We have used the very same water with minimal additions (resulting from maintenance and replacement of models) for the past six years. The only maintenance issue is the tendency of minute fraction (10^{-4} molar) of the I^- ions to turn to I^{-3} in the presence of Oxygen and light. The latter absorbs green light, preventing PIV measurements. To solve this problem, we keep the facility oxygen free by pumping the air out, and by injecting N_2 to the gas chamber in the pressure control tank. This procedure is repeated about once a week. During model replacements, we store the liquid briefly in a separate tank and return it back to the facility. Any effect of exposure to oxygen is reversed by de-aeration and exposure to N_4.

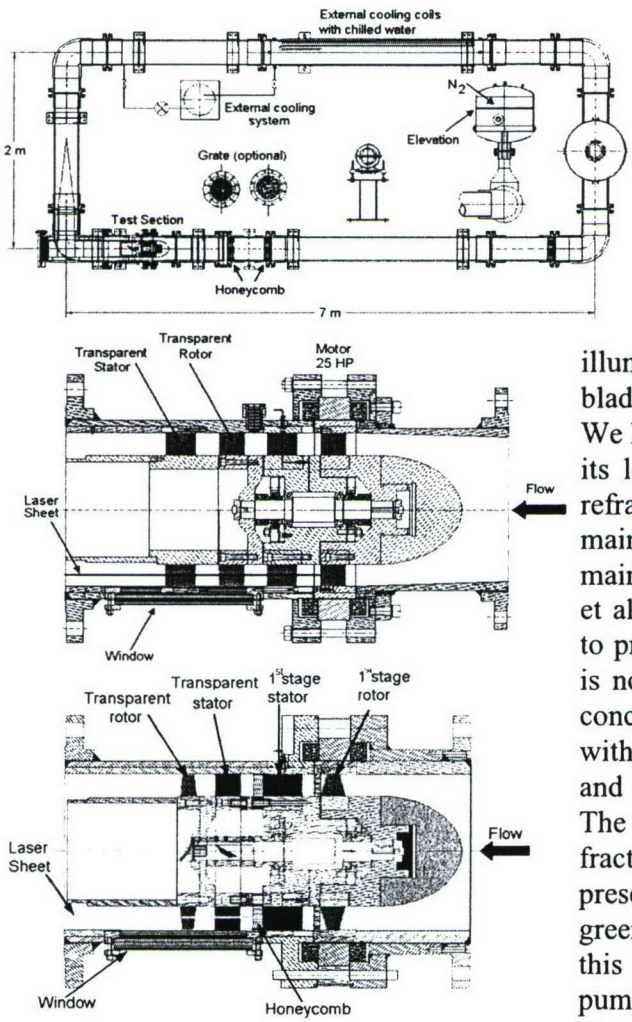

Figure 3.1: (a) The axial turbomachine facility, (b) test setup No. 1, and (c) test setup No. 4.

Table 1

	Test Setup	
	No. 1	No. 2
No. of stages	2	
No. of rotor blades	12	
No. of stator blades	17	
Hub-to-tip ratio	0.708	
R2-S2 axial gap/Rotor axial chord	1.92	1.41
S1-R2 axial gap/Rotor axial chord	1.95	N/A
Rotor pitch-to-chord ratio (mid-span)	1.34	1.34
Stator pitch-to-chord ratio (mid-span)	0.66	0.97
Rotor chord (mm)	50	50
Stator chord (mm)	73.2	50
Rotor and Stator span (mm)	44.5	44.5

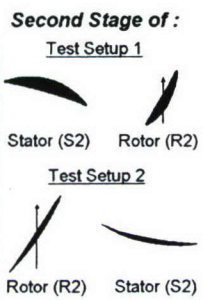

The test facility was constructed using funding provided in part by AFOSR and in part by ONR. Two different test setups have been utilized. Setup No. 1 (Fig. 3.1b), has an aircraft compressor like

arrangement, and has 4 blade rows constituting two identical stages. The window covers the entire second stage. The main geometrical parameters of this axial-turbo-pump are listed in Table 1. Additional relevant parameters are a rotor blade thickness of 7.62 mm, and camber varying from 4.54 mm at the hub to 1.98 mm at the tip. The stators blade thickness is 11 mm and its camber is 6.22 mm. The gap between the rotor and the stator is variable. In many prior experiments, a constant gap of 50 mm was used. Recently, we reduced the gap between the second rotor to the second stator to 14 mm, 28% of the rotor chordlength, in order to increase the blade-row interactions and associated deterministic stresses. Specific objectives associated with this setup are discussed in Section 4.

In test setup No. 2 the first stage (rotor and stator) is identical to that of setup No. 1. However, the second stage consists of a stator (IGV) followed by a rotor. A 10 mm long honeycomb with 1.58 mm opening is installed downstream of the first stage in order to reduce the effect of wakes and secondary structures generated by the first stage, and to align the flow in the axial direction, consistent with the orientation of the first stator. The gap between the honeycomb and the second stage stator is 22 times the honeycomb openings, sufficient for eliminating wakes of individual honeycomb elements, as prior measurement have indicated. The IGV has 17 blades, each with a chordlength of 73.2 mm and span of 44.5 mm. The rotor has 12 blades, each with a chordlength of 50 mm and span of 44.5 mm. This setup provides substantially reduced effects of the first stage, and as a result, a clearer picture on interactions between the IGV wakes and the rotor blade, as described in Section 4.

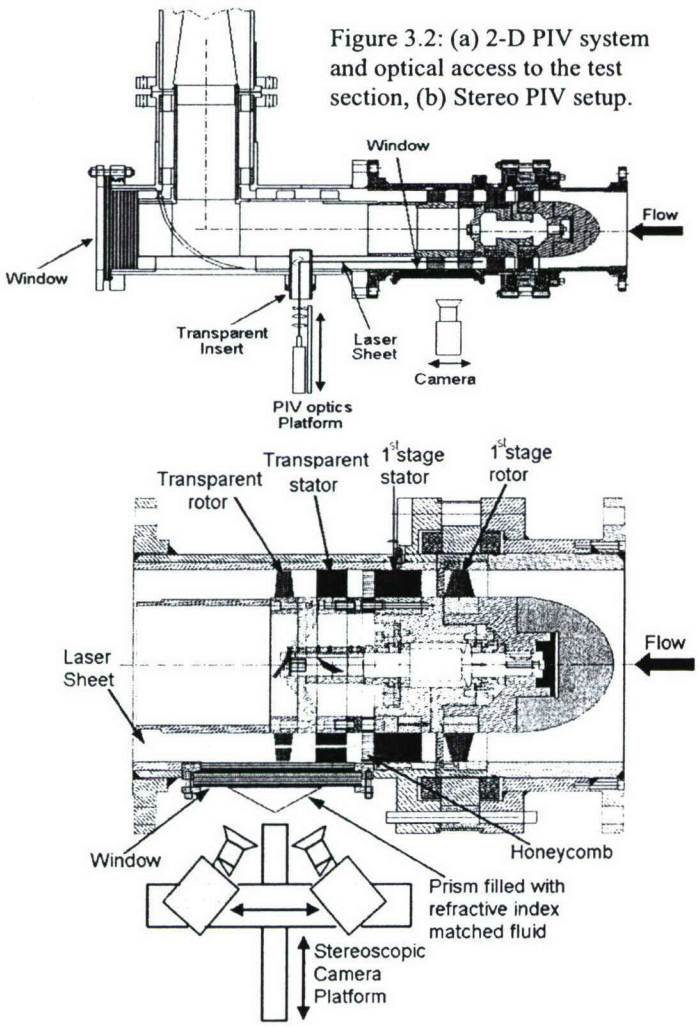

Figure 3.2: (a) 2-D PIV system and optical access to the test section, (b) Stereo PIV setup.

The blade rows have been precision-manufactured using five axis CNC machines. The system is driven by a 25 HP, rim driven motor, which drives the first rotor directly, and is connected to the second rotor through a shaft mounted on precision bearings. Most of the previous measurements have been performed at a rotor blade speed of 500 rpm, i.e. the Reynolds number based on the rotor tip speed and chordlength is 3.7×10^5.

3.2 PIV Setup & Experimental Procedure

Optical access is provided by a window that extends from upstream of the rotor, covers the entire 2nd stage and terminates downstream of the stator (Figures 3.1, 3.2). An additional transparent insert enables us to insert a probe containing the laser-sheet optics. Figure 3.2a illustrates the 2-D PIV setup, which enables us to

measure the two in-plane velocity components (u_1, u_2), and Figure 3.2b shows the stereo PIV setup, which enables measurements of all three velocity components in planes extending from the hub up to very close to the tip of the blades (up to r/r_{tip}=0.97). In Section 3.3 we also introduce stereo-PIV measurements in planes aligned perpendicularly to the mean flow in order to probe the flow in the tip region.

The light source of the PIV system is a dual-head Nd-YAG laser, whose beam is expanded to generate a 1 mm thick light sheet. The flow is seeded using 20% silver coated, hollow glass, spherical particles, which have mean diameter of 13μm (smaller particles are also available) and an average specific gravity of 1.6, i.e. slightly below that of the working fluid. The images are recorded by a 2048×2048 pixels^2, Kodak ES4.0, 8-bit, interline transfer digital camera and stored. We have recently purchased a pair of higher quality, 14 bit, 2048×2048 pixels^2 digital cameras from La Vision and a mass data acquisition system that will be used in future studies. The laser and the camera are synchronized with the orientation of the rotor using a shaft encoder that feeds a signal to a controller containing adjustable delay generators. Consequently, we can acquire data at any desired rotor phase.

To obtain converged turbulence statistics, we record 1000 instantaneous images at the same phase. The sample area varies, depending on the desired resolution. For most cases, the instantaneous field of view varies from 15x15 to 50x50 mm^2, and the vector spacings vary between 100 - 400 μm, depending on the desired resolution. Smaller vector spacing, below 50 μm, is also possible, if needed. We frequently have to combine data from several locations to obtain the entire desired field of view. Data analysis includes image enhancement and cross-correlation analysis using in-house developed software (Roth et al., 1999, 2001, Chen et al., 2005b). The stereo-data is matched to obtain the out-of-plane component using software/procedures provided by Dantec Inc. Adapting these procedures to the current geometry, including image enhancement procedures, is discussed in Uzol et al. (2002a). The typical uncertainty in instantaneous displacement is ~0.3 pixels, provided the window contains at least 5-10 particle pairs. For a typical displacement between exposures of 20 pixels, the resulting uncertainty in instantaneous velocity is 1.5%. Slip due to the difference between the specific gravity of the particle and fluid is negligible (<0.2%, Sridhar & Katz, 1995). The uncertainty in phase-averaged results is lower, since the error is inversely proportional to the square root of the number of samples.

4. Summary of Accomplishments During the Present Grant

This section briefly summarizes some of our progress over the past three years. A complete picture is provided in a series of journal and conference publications (Uzol et al., 2001, 2002a,b,c, 2003a, b, 2004a, b, 2005a, b, 2007; Chow et al., 2002a, b, c, 2003a, b, 2005a, b), Brzozowski et al., (2005) and Soranna et al. (2004, 2005a, b, 2006a, b, c, d, e, 2007a, b). For the Soranna et al. (2005b) paper, we have received the Knapp Award for the best paper presented in the ASME, Fluids Engineering Division Summer Meeting (2005).

4.1 Stereo PIV data in the Rotor Near wake

Figure 4.1 shows sample phase-averaged, 3-D velocity distributions and turbulent kinetic energy (Uzol et al., 2004a, b) behind a rotor blade (setup No. 2, Fig. 3.1). To obtain these distributions, we have performed stereo PIV measurements in numerous (x,y) (or (x_1,x_2)) planes. At 50-55%

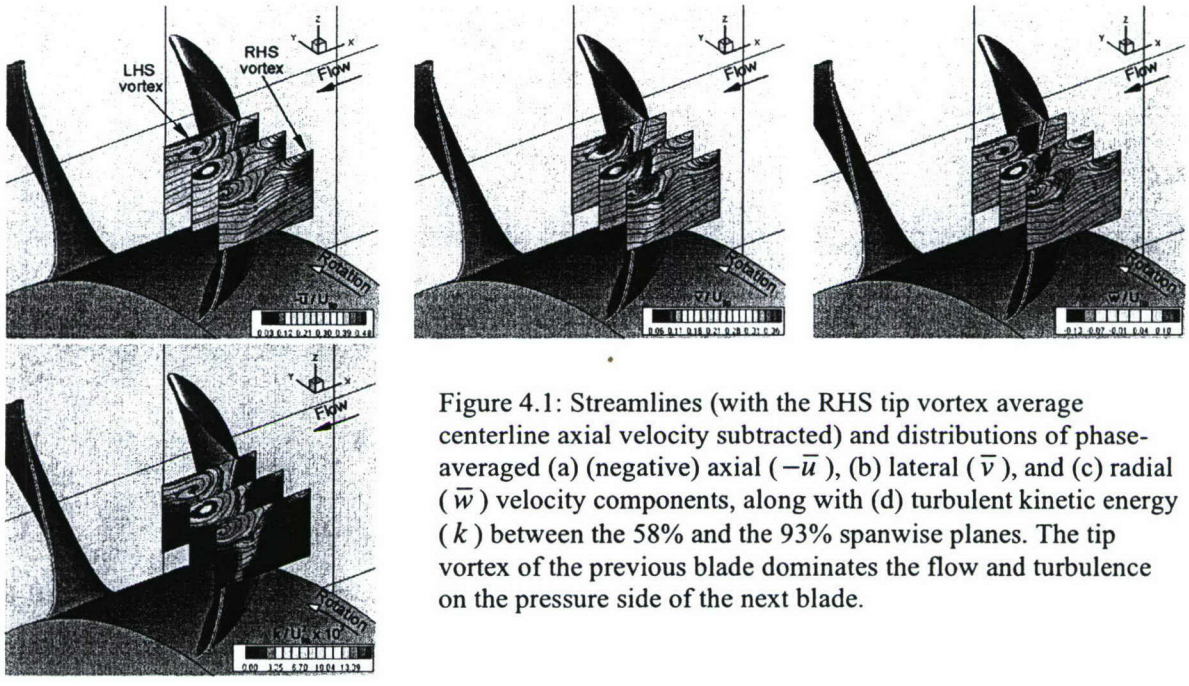

Figure 4.1: Streamlines (with the RHS tip vortex average centerline axial velocity subtracted) and distributions of phase-averaged (a) (negative) axial ($-\overline{u}$), (b) lateral ($\overline{v}$), and (c) radial ($\overline{w}$) velocity components, along with (d) turbulent kinetic energy (k) between the 58% and the 93% spanwise planes. The tip vortex of the previous blade dominates the flow and turbulence on the pressure side of the next blade.

and 88-93% of the span, the data are acquired in 10 very closely spaced radial planes, every 0.25 mm, i.e. less than the light sheet thickness. This procedure enables us to calculate the 3-D phase-averaged vorticity and all the components of the strain-rate tensor. Additional data are obtained in more sparsely separated planes over the entire span.

In the tip region, interaction of the tip vortices with the blades dominates the flow. The rotor is confined between two tip vortices; one that rolls up from the same blade that generates the wake, located to the right of the blade, and the other that rolls up from the previous blade, located to the left of the blade. The velocity field induced by the latter tip vortex and entrainment of the casing boundary layer reduce the axial velocity, mostly above the vortex. The previous tip vortex also induces negative radial velocity in the gap between its core and the pressure side of the subsequent blade. Thus, the previous tip vortex greatly affects the vortex rollup in the next blade, preventing rollup near the trailing edge, i.e. rollup of a tip vortex is pushed further upstream. The high lateral/circumferential velocity in the vortex core is associated with entrainment of the blade boundary layer. These phenomena are striking examples of interaction between blades of the same row. The tip vortex also generates high turbulence along the rotor pressure side, due to the entrainment of the blade and casing boundary layers, and due to passage near the pressure side of the blade, which alters the vortex trajectory, causes meandering and sometimes bursting. Analysis of the characteristics of Reynolds stresses, along with the associated production, diffusion, dissipation and advection rates in the tip region is still in progress.

The effects of the tip vortices diminish below 75% of the span. The radial velocity becomes much lower than the axial and lateral components, and the radial vorticity component becomes dominant. However, the axial and lateral vorticity components are not negligible, i.e. the flow is three-dimensional. In § 4.4, we use the mid-span data to examine the evolution of Reynolds stresses in the near rotor wake.

4.2 Structure and turbulence within a wake generated by an upstream IGV blade as it impinges on a rotor blade and passes within a rotor passage:

In this Section we examine the changes to the flow structure and Reynolds stresses as a wake, generated by an upstream stator or Inlet Guide Vane (IGV), interacts with a rotor blade and propagates through a rotor passage. Changes to mean flow and Reynolds stress within this IGV wake are examined using high-resolution PIV measurements at six rotor blade phases (2D in this case), three focusing on the rotor leading edge, and the others on the vicinity of the trailing edge. The discussion here focuses mostly on the turbulence parameters. The substantial changes to flow and pressure gradients around the rotor leading edge are discussed briefly, but are addressed in detail in Soranna et al. (2005a, 2006a, c).

Due to spatially non-uniform velocity distribution, especially on the suction side, the wake deforms while being advected around the blade, expanding near the leading edge and shrinking near the trailing edge. A geometrically correct sketch, and sample phase average vorticity distributions showing these trends are presented in Figure 4.2. The wake broadens near the leading edge due to differences between the velocity in its forward side, and the near stagnation flow (in the rotor reference frame) on its back side. As the wake widens, the phase averaged velocity gradients at the center of the wake diminishes, leaving a substantial region at the center of the wake with almost zero mean vorticity. Near the trailing edge the wake compresses due to the adverse velocity gradients on the aft side of the rotor blade.

Impingement exposes the IGV wake to a phase-dependent strain field generated by the rotor blade. As a result, the turbulence becomes highly non-uniform and anisotropic. Figure 4.3 presents the distributions of phase-averaged axial, $-\overline{u}$ (in the context of RANS, an overbar or brackets $\langle ... \rangle$ will be used interchangeably to denote phase averaging), and lateral velocity components, this time in the rotor reference frame, $\overline{v_r}$, along with the turbulent kinetic energy, as the IGV wake is chopped off and sweeps across the rotor blade. In these plots, the rotor leading edge is located at $(x/c,y/c)=(0,0)$. For each phase, two adjacent 15x15 mm^2 sample areas are needed to cover the flow field around the rotor leading edge. The location of the IGV wake in each phase can clearly be identified in the turbulent kinetic energy plots. In Phase 1 (top row), the IGV wake center is located above the rotor leading edge. In Phase 2 (middle row), the IGV wake center is impinging on the leading edge, and in Phase 3 (bottom row), the center of the wake intersects with the rotor blade at about 20% of the rotor chordlength.

In Soranna et al. (2006a) we show that wake impingement causes 9% changes in phase averaged

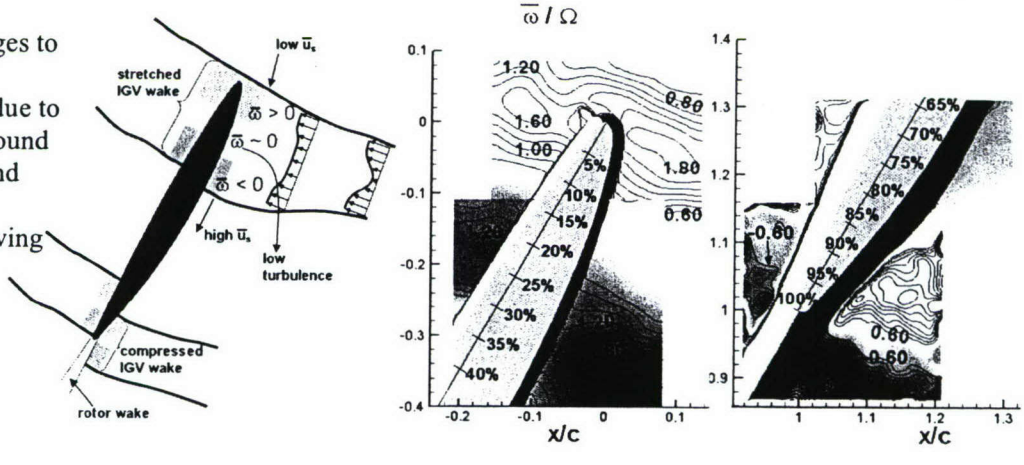

Figure 4.2: Changes to dimensions of impinging wake due to the strain field around the rotor blade, and sample vorticity distributions showing these trends.

relative lateral velocity, and that the distributions of axial velocity on the suction side display clear effects of wake deficit, i.e. a decrease on $-\bar{u}$ within the wake. On the pressure side of the blade, the phase-dependent variations in $\overline{v_r}$ and $\bar{u}$ are equally severe, but their trends differ due to differences in advection speed. These trends cause significant phase-dependent changes to blade loading, as manifested by distributions of wall-parallel velocity gradients, $\partial \overline{u_s} / \partial s$, where s is the wall-parallel curvilinear coordinate. Thus, $\bar{u}_s \partial \bar{u}_s / \partial s$, a key contributor to pressure gradients along the wall, is strongly phase dependent.

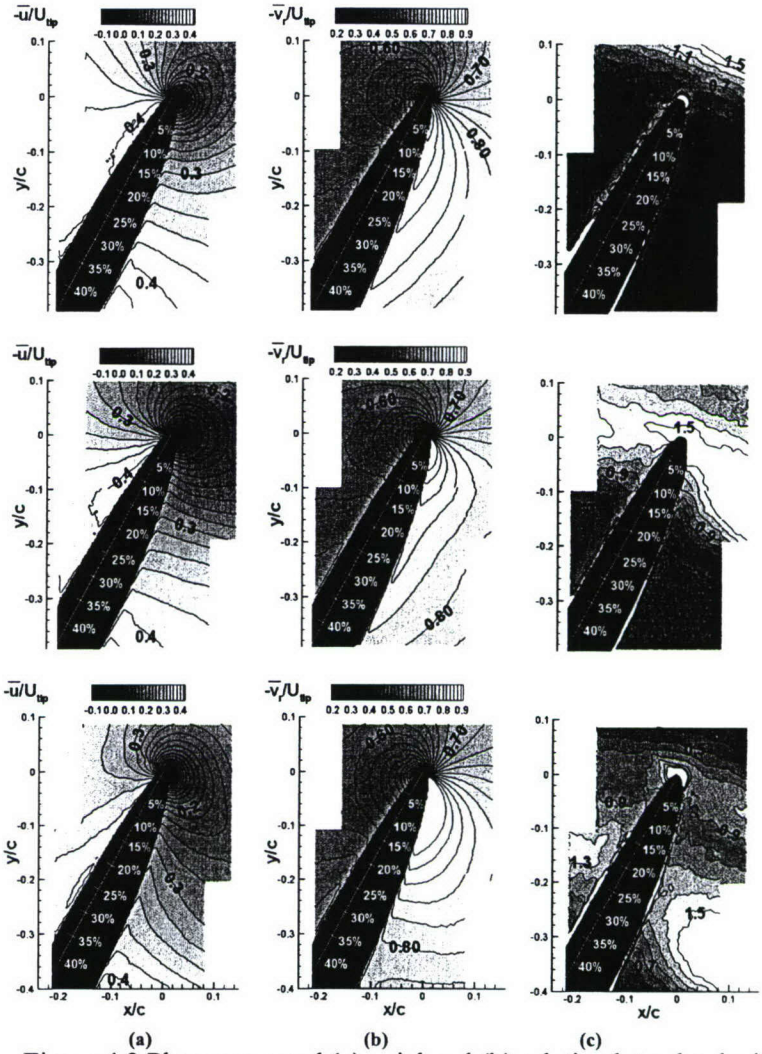

Figure 4.3 Phase-averaged (a) axial and (b) relative lateral velocity components; (c) turb. kinetic energy near the rotor leading edge at mid-span. Top: phase 1, Middle: phase 2, Bottom: phase 3

Figures 4.4 and 4.5 show the distribution of normal Reynolds stresses in wall-parallel ($\overline{u_s'^2}$) and wall-normal ($\overline{v_n'^2}$) directions within the same impinging wake, near the leading edge in phases 1 – 3, and near the trailing edge in phases 4 - 6. A few of the perplexing phenomena include a substantially higher velocity fluctuations in phases 4-6 (compared to phases 1-3), the increase of the wall-parallel component and decrease of wall-normal component near the leading edge of the blade, and the complex distribution of both normal stress components in phase 3. To explain these phenomena, we will relate the distribution of the Reynolds stresses to the magnitude and orientation of the principal strain field in different regions. Figure 4.6 is introduced to illustrate the principal strain orientations in several regions of interest, and will be referred to often in the following discussions.

Effect of Streamwise Diffusion: Axial turbomachines rely on aerodynamic diffusion to achieve pressure rise in the aft part of a vane passage. This diffusion process increases the compressed streamwise velocity fluctuations and suppresses the extended wall-normal fluctuations, consistent with predictions of Rapid Distortion Theory (RDT, Batchelor, 1954; Chen et al.,

2005s, 2006; De La Riva et al., 2004). The present distributions of normal stresses are consistent with the trends predicted by RDT.

For example, starting with phases 4 - 6, $\overline{u_s'^2}$ increases and $\overline{v_n'^2}$ decreases in the diffusion dominated region, in the aft part of the rotor blade passage. This region is characterized by $\partial \overline{u_s} / \partial s < 0$, i.e. the mean flow is compressed in the streamwise direction and extended in the normal direction (region 1 in Figure 4.6). An increase in streamwise component can also be predicted by examining the relevant production terms in the Reynolds Stress Transport Equations (Pope, 2000). In the diffusion region (#1, Figure 4.6), $-\overline{S_{ss}}\,\overline{u_s'^2}$ is positive and large ($\overline{S_{ij}}$ is the phase averaged strain rate), contributing to an increase in streamwise fluctuations, whereas $-\overline{S_{nn}}\,\overline{v_n'^2}$ is negative, indicating a decrease in the wall-normal turbulence level. Away from the wall, s and n are almost aligned with the principal directions, and the values of $\overline{u_s' v_n'}$ are small. Thus, only normal components contribute significantly to the production rate.

Due to the diffusion in the previous passage, the IGV wake turbulence arriving in phases 1 and 2 must already have elevated $\overline{u_s'^2}$ and suppressed $\overline{v_n'^2}$, as is evident from the phase 2 data, especially near and to the left of the pressure side of the blade. On the pressure side, this trend persists also in phase 3, but the picture becomes more complicated due to leading edge effects discussed below.

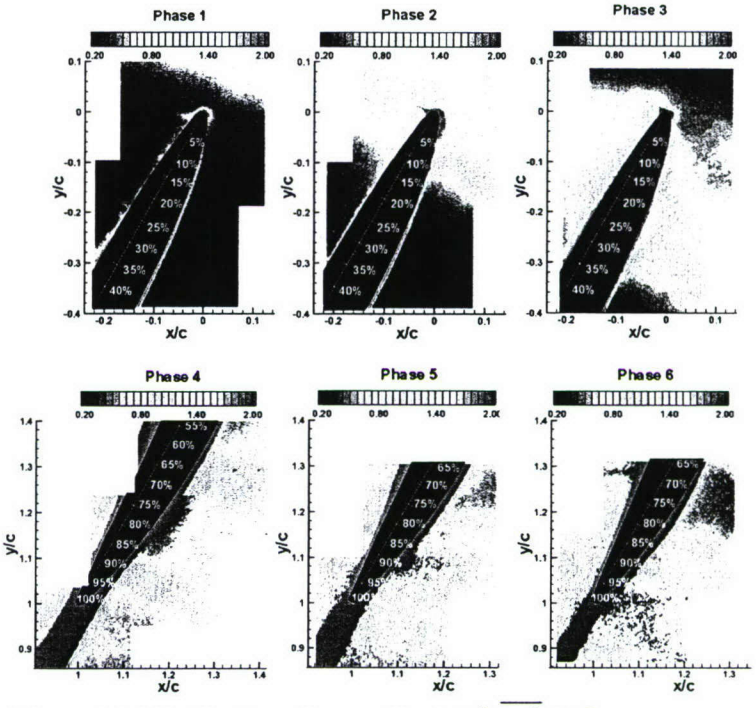

Figure 4.4. Distribution of normalized $10^3 \cdot \overline{u_s'^2} / U_{tip}^2$

Top row: phases 1 - 3 (leading edge region).
Bottom row: phases 4 to 6 (trailing edge region).

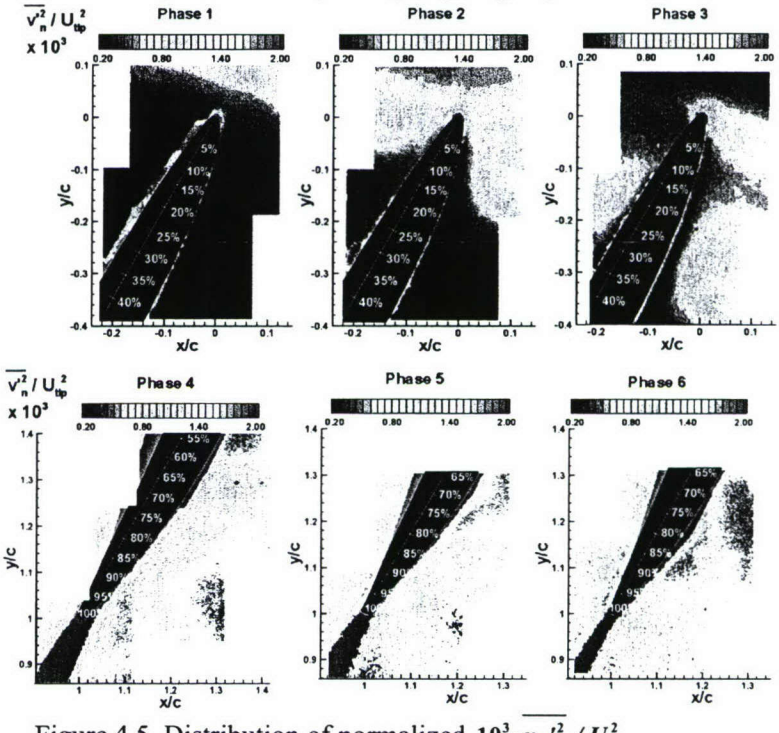

Figure 4.5. Distribution of normalized $10^3 \cdot \overline{u_n'^2} / U_{tip}^2$

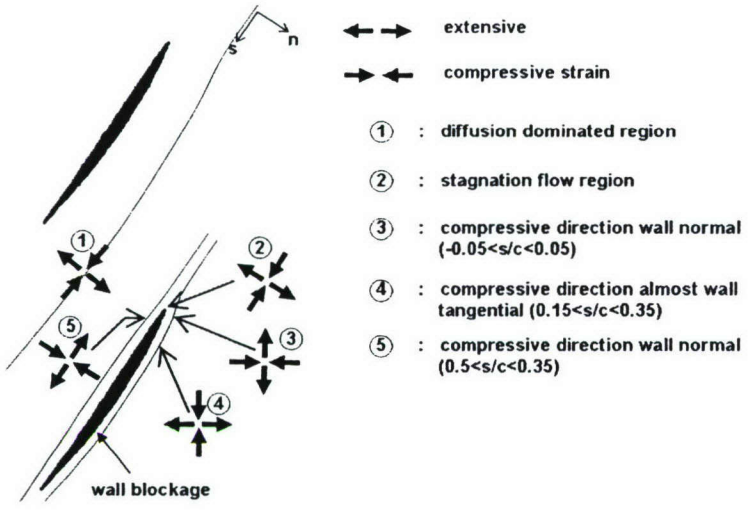

Figure 4.6. The orientation of the principal phase averaged strain eigenvectors in within the rotor passage.

Effect of straining: Following the same logic, the streamwise fluctuations should be suppressed in a region with $\overline{S_{ss}}>0$, i.e. when the wall-parallel component is stretched. Since the dominant phase averaged variations in flow at mid span is almost two dimensional, axial stretching is accompanied by normal compression, $\overline{S_{nn}}<0$, and an increase in the wall-normal turbulence. To demonstrate this trend in the present data, let's focus on the region with elevated wall-normal Reynolds stress in phase 3, between s/c=-0.05 and s/c=0.05 on the suction side (#3 in Figure 4.6). In the same region the streamwise turbulence intensity is considerably reduced. In order to support this claim, Figure 4.7 shows the distributions of the compressive, $\overline{S_c}$, and extensive, $\overline{S_e}$, mean principal strain rates. The arrows in each figure indicate the principal directions of compression and extension. In region 3, the principal direction of compression is aligned with the wall-normal direction. Thus, the compressed, wall-normal fluctuations should increase, while the stretched wall-parallel fluctuations should decrease. If we project the Reynolds stress tensor onto a coordinate system aligned with principal strain directions (Figure 4.8), in region 3, $\overline{u_c'^2}$ (stress aligned with the compressive strain eigenvector) is significantly larger than $\overline{u_e'^2}$ (stress aligned with the extensive strain eigenvector). As expected, the turbulence is enhanced along the principal direction of compression.

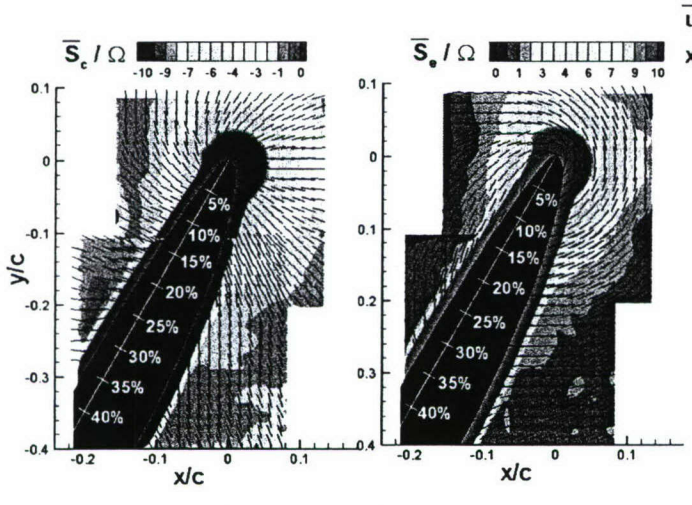

Figure 4.7: Distributions of the most compressive mean strain eigenvector, $\overline{S_c}$, and most extensive strain eigenvectors, $\overline{S_e}$.

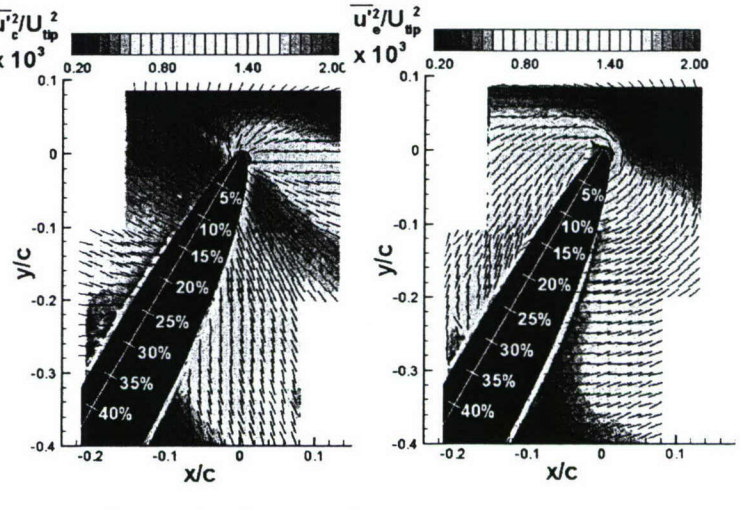

Figure 4.8: The normal Reynolds stresses components in the most compressive, $\overline{u_c'^2}$, and extensive $u_e'^2$ strain eigen-directions.

With reference to Figure 4.8, one can also see that on the suction side, in the 0.15<s/c<0.35 region (#4, Figure 4.6), the principal directions of compression and extension are rotated about 90° compared to their orientation in region #3. Thus, in this area, the compressive strain rate is almost aligned with the streamwise direction, namely $\overline{u_s'^2}$ should increase, and the (stretched) $\overline{u_s'^2}$ should be suppressed. Indeed, in this region $\overline{u_s'^2} > \overline{v_n'^2}$. Furthermore, when projected onto the principal directions of strain, Figure 4.8 shows that $\overline{u_c'^2} > \overline{u_e'^2}$. However, the strain rates in this region are lower than those at the leading edge. Therefore, the effect of straining on turbulence production must diminish, and may be overwhelmed by another mechanism, e.g. advection of turbulence generated before.

Along the pressure side of the blade (#5 in Figure 4.6), the direction of compression is normal to the wall while the extension is oriented in the streamwise direction. In spite of these trends $\overline{u_s'^2} > \overline{v_n'^2}$, in contrast to the expected local production and/or RDT predictions. To explain this contradiction, note that the strain rates on the pressure side are lower than those on the suction side, i.e. the turbulence production rate is lower. Furthermore, as noted before, the IGV wake segment propagating along the pressure side has already experienced the effects of diffusion (region 1), which enhances the streamwise component and suppresses the normal fluctuations. The local production is too weak to overcome the effects of prior diffusion.

Effects of wall blockage: The turbulence near the blade is additionally modified by the 'wall blockage' phenomenon, which suppresses the wall-normal turbulence, and increases in the wall-parallel fluctuations (Perot & Moin, 1995; Hunt & Graham, 1978; Uzkan et al., 1967; De La Riva et al., 2004). Wall blockage causes inter-component turbulent kinetic energy transfer from the wall-normal to the wall-parallel component, mostly due to the effect of the pressure strain term in the Reynolds Stress Transport Equations. The present distributions in phase 3 clearly demonstrate suppression of the wall-normal component and enhancement of the wall-parallel component in thin layers located near the wall but outside of the boundary layer, especially in the 0.15<*s/c*<0.3 region. One can also observe the effects of wall blockage on the near-wall turbulence in phases 4-6, especially along the suction side of the blade.

Effect of non-uniform production rate: Still focusing on phase 3, one cannot avoid noticing the region with low turbulence between *s/c*=0.05 and *s/c*=0.15, on the suction side of the blade (Figures 4.4, 4.5, 4.8). This area is located in the middle of the impinging wake. To explain this trend, we calculate the distribution of production and show that it is negative, i.e. the local non-equilibrium conditions cause transfer of energy from the turbulence to the mean flow. Neglecting out of plane effects (reasonable at mid span), the in-plane contribution to production is $P_{2D} \approx -\overline{S_c}\,\overline{u_c'^2} - \overline{S_e}\,\overline{u_e'^2}$. Since $\overline{S_c} \approx -\overline{S_e}$, $P_{2D} \approx \overline{S_e}(\overline{u_c'^2} - \overline{u_e'^2})$. The distribution of production, along with the components contributing to it are presented in Figure 4.9. The production can be positive or negative depending

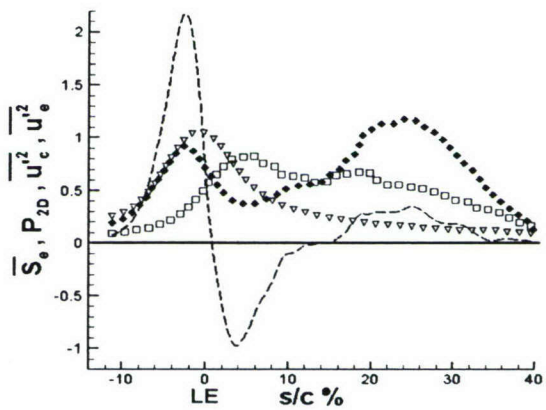

Figure 4.9. Wall-parallel distributions of: $\overline{S_e}$ (∇), $\overline{u_c'^2}$ (♦), $\overline{u_e'^2}$ (□), – – turbulence production along a streamline located 0.03C from the suction surface.

on the relative magnitude of $\overline{u_c'^2}$ and $\overline{u_e'^2}$. In equilibrium conditions, $\overline{u_c'^2} > \overline{u_e'^2}$, due to the compression effect. Negative production would occur under non-equilibrium conditions, e.g. when the direction of strain changes rapidly, while the turbulence requires time to respond. In such a case, $\overline{u_e'^2} > \overline{u_c'^2}$ locally and the production becomes negative. In the present flow, the negative production at $0.01 < s/c = 0.15$ is almost coincident with the low turbulence region in the transition between regions 3 and 4 (Figure 4.6), where the directions of compression and extension switch by almost 90° (Figure 4.7).

4.3 RANS Simulations of an Entire Stage

Non equilibrium phenomena that have substantial effects on the turbulence production near the leading edge, as well as in other regions with rapid changes to the stain field, are very difficult to model in RANS simulations. They cannot be accounted for by the popular eddy viscosity (e.g. k-ε) models due to incorrect modeling of the production term in the k equations. Consequently, RANS simulations are notorious for overproducing turbulence near the leading edge of lifting surfaces (see Durbin 1996). Indeed, RANS simulations of the flow in our facility (setup No. 1, figure 3.1, Brzozowski et al., 2005; Uzol et al., 2007), using several turbulence models, substantially overproduce turbulence, especially near the leading edge, and over expand wakes. Due to previous lack of data, these simulations are the first attempt to compute the flow over an entire turbomachine stage, where a complete database is available for benchmarking. We have also used measured inflow and distribution of Reynolds stresses as boundary conditions. Such data are essential for development and benchmarking turbulence models within turbomachines.

We have focused on the flow conditions at mid-span, where the experimental flow is almost (but not entirely) 2D. Three standard RANS models have been considered: (a) k-ε model with the standard constants, (b) RNG k-ε model, and (c) a full Reynolds stress transport model (Launder 1989) with the turbulent diffusion model of Lien & Leschziner (1994). A commercial grid-generator (GAMBIT™) is employed, and the equations are solved using a commercial CFD code (FLUENT™). The domain consists of the 17 stator blades, and 12 rotor blades, separated by a sliding line. Inlet conditions are matched to the PIV data at the rotor inlet. The mesh contains a total of 3×10^5 cells, and there are 40 time-steps per rotor passage (480 time-steps per revolution), and we run the simulation for 800 time-steps (20 rotor passages) to obtain a periodic solution. Figure 4.10 compares the modeled (RNG k-ε, and RANS with full Reynolds stress transport equation) to the measured, phase-averaged absolute velocity angle. The angle is measured in the

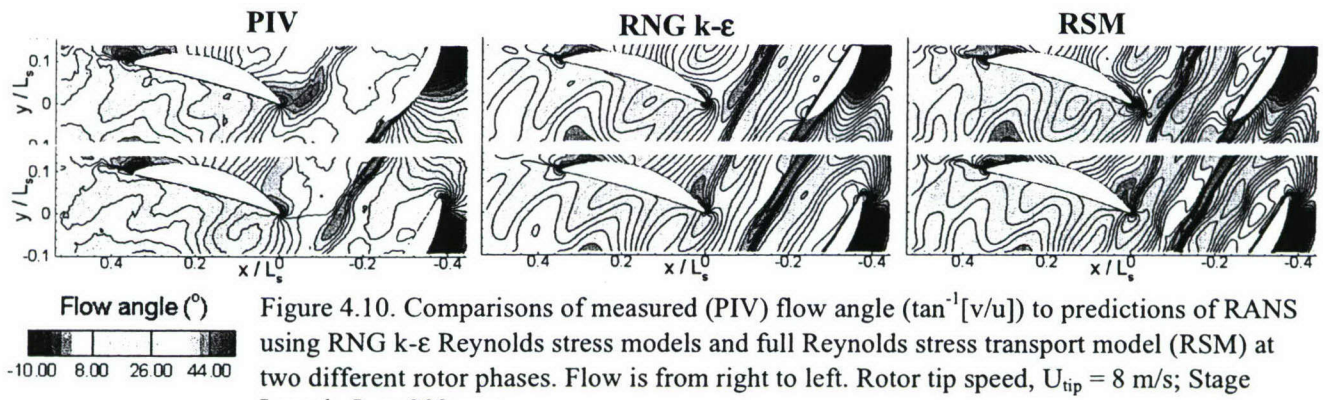

Figure 4.10. Comparisons of measured (PIV) flow angle ($\tan^{-1}[v/u]$) to predictions of RANS using RNG k-ε Reynolds stress models and full Reynolds stress transport model (RSM) at two different rotor phases. Flow is from right to left. Rotor tip speed, U_{tip} = 8 m/s; Stage Length, L_s = 203 mm.

clockwise direction with respect to the streamwise direction (from right to left). As can be seen, overall features of the mean flow angle appear quite well predicted by the RANS. However, significant differences occur in some important details, such as rotor wakes being more diffused in the experimental data as compared to the RANS.

Next, we are interested in establishing whether the different models are able to reproduce the characteristic lattice of wakes with elevated turbulent kinetic energy observed in the experimental data, and their spatial distribution. Figures 4.11 show the results, covering an entire

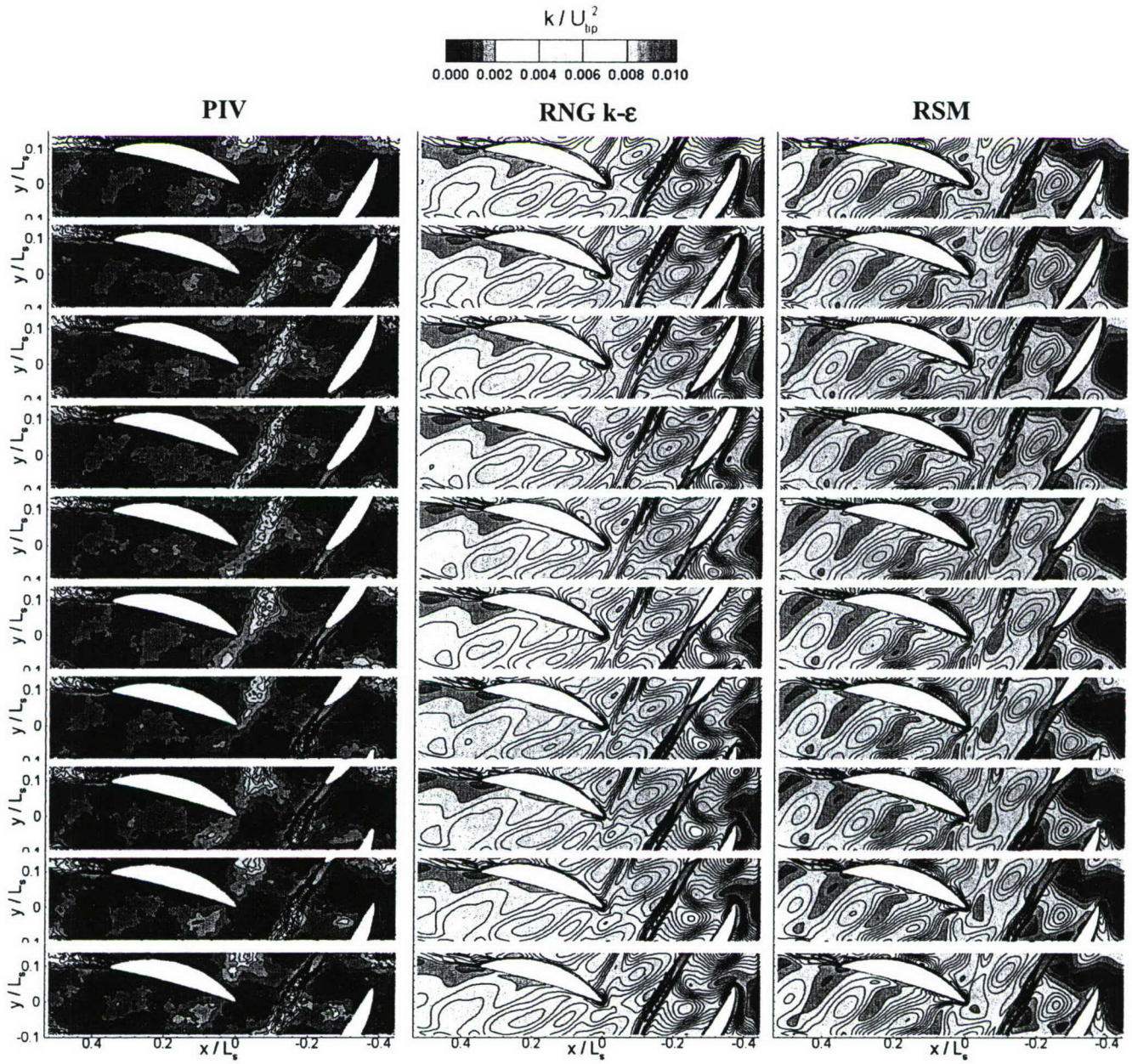

Figure 4.11. Comparison of measured turbulent kinetic energy (k) to predictions of RANS using RNG k-ε Reynolds stress models and full Reynolds stress transport model (RSM) at ten different rotor phases for ten different rotor phases covering and entire blade passing period. Flow is from right to left.

rotor passage cycle, and compares them to the experimental data. As is evident, some features are reproduced, but others are not. The overall level of turbulent kinetic energy is clearly over-predicted in the RANS. The RNG k-ε model overpredicts k at the leading edge of the rotor, where TKE production may be over-predicted due to the eddy-viscosity assumption in conjunction with the rapid straining there. Such excessive production is much more accentuated in the standard k-ε (not shown), where significant kinetic energy is produced even at the leading edge of the stator, which does not occur in the PIV data.

The full Reynolds stress transport model also substantially over-produces turbulence both near the leading edge and within the blade passage, but not to the same extent as the RNG k-ε model. One of the likely contributor to the discrepancy, even in the full Reynolds Stress Transport model, is the improper predictions of pressure-velocity correlations and pressure strain in evolution equations of Reynolds stresses. Note that our objective is not to downplay the significance/ability of RANS simulations; we only wish to point out that there are still many unresolved issues in highly strained flows.

4.4 The structure of turbulence within a sheared rotor wake:

As discussed in detail in Soranna et al. (2005b, 2006b, d), chopping and variations of advection speed of the upstream IGV wakes, as they pass along the rotor blade, create a non-uniform flow that shears the rotor wake. Due to the overwhelming effects of the non-uniform strain field, the trends of the Reynolds stresses within the sheared wake differ significantly from those measured in previous studies of curved wakes (e.g. Weygandt & Metha 1995; Koyama, 1985; Nakayama, 1987; Hah & Lakshminarayana, 1982; Ramjee & Neelakandan, 1989; John & Schobeiri, 1996). The discrepancy in trends between the classical curved-wake data on the present results is illustrated in Figure 4.14. As is evident, in a typically curved wake, the turbulence is enhanced (mildly) in the inner side of the wake, whereas in the present data, the turbulence is clearly enhanced significantly on the outer side. The picture is actually much more complicated. As illustrated by the distributions of all the six Reynolds stresses presented in Figure 4.13, the present axial velocity fluctuations increase along the suction/outer side of the wake, while the circumferential component decays. On the pressure/inner part of the wake the circumferential velocity fluctuations are higher. Furthermore, the distributions of Reynolds shear stresses display high inhomogeneity and anisotropy, but they are consistently higher on the suction/outer side.

To explain the present trends and the differences from prior studies, we have examined the distributions of Reynolds stresses and production rates in two coordinate systems, the first aligned with the principal strain directions, and the second is a curvilinear system (s,n), aligned with the wake centerline. The analysis in principal strain coordinate system demonstrates that changes in the direction and magnitudes of compression and extension, and the resulting spatial variations in turbulence production rate, fully explain the spatial variations in Reynolds stress components (Soranna et al., 2006b, not shown here). To explain the differences from prior studies of curved wakes, in Figure 4.14 we show a sample distribution of turbulent kinetic energy and the term contributing to its evolution. A complete analysis of all the Reynolds stress components at several sections across the wake is provided in Soranna et al. (2006b). Following So & Mellor (1972), Bradshaw (1973), and Weygandt & Metha (1995), but including all terms (except for a negligible Coriolis force contribution), the transport equations of turbulent kinetic energy in the (s,n) system is

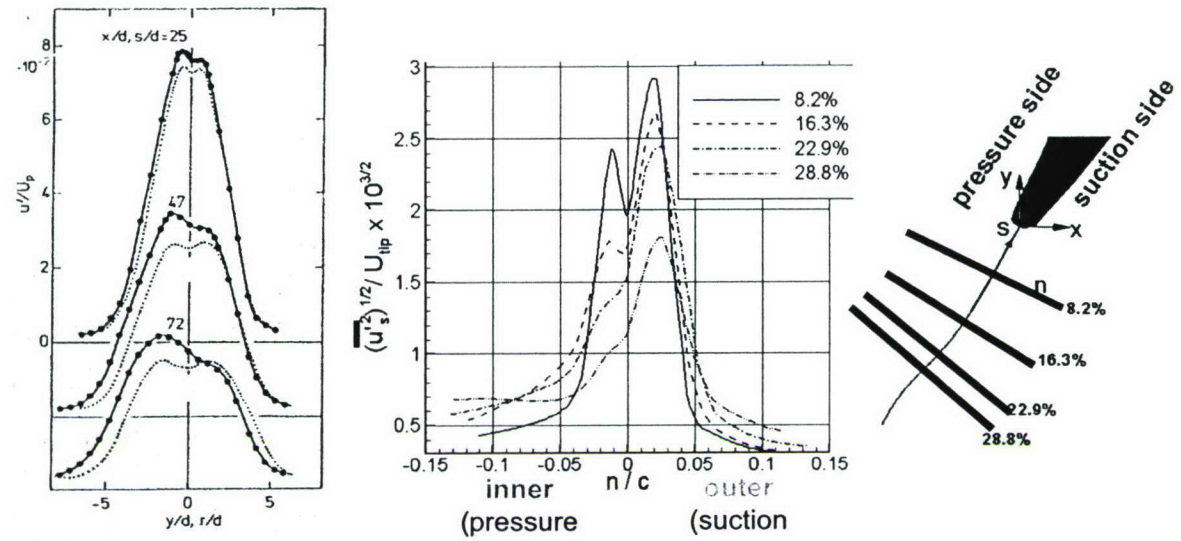

Figure 4.12: A comparison between trends of streamwise velocity fluctuations in a classical curved wake data (left side, Koyama, 1983) and the present sheared rotor wake (right side).

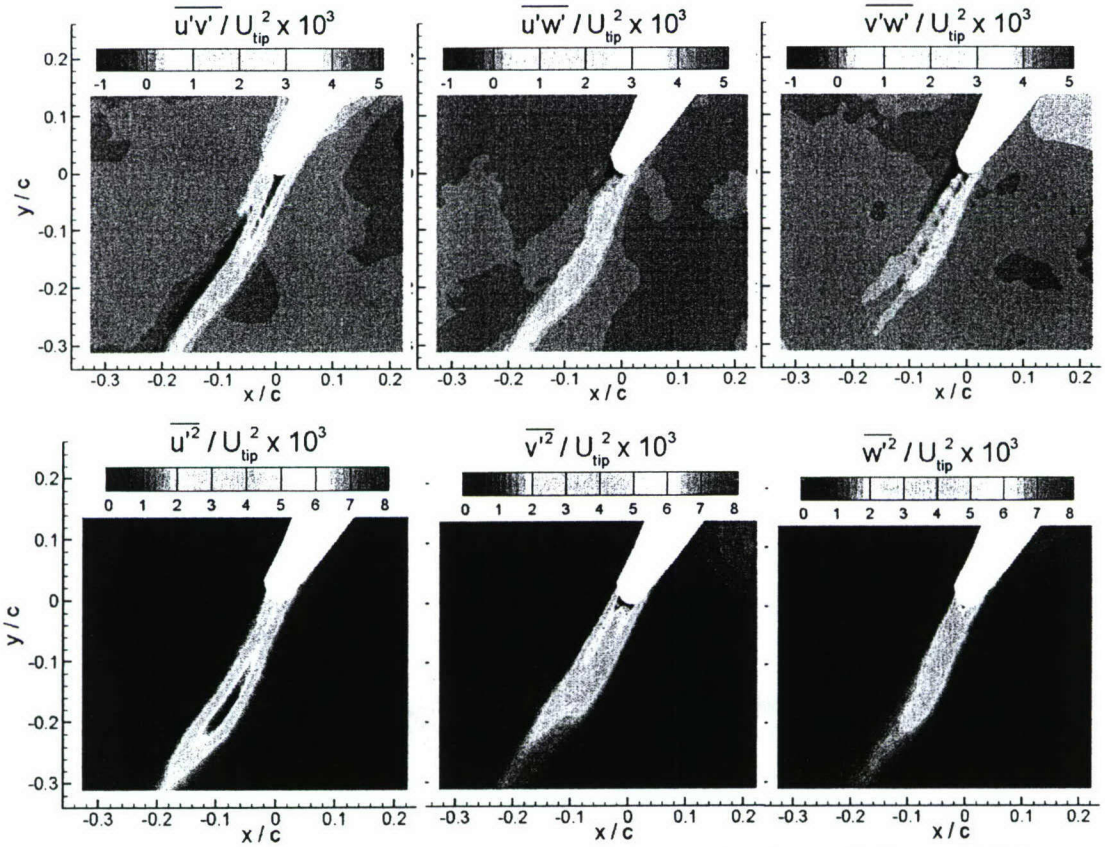

Figure 4.13: Reynolds stresses in the sheared near rotor wake. Setup #2, Stereo PIV data.

$$\frac{\partial}{\partial t}(k) = -\left[\frac{1}{h}\overline{U_s}\frac{\partial}{\partial s} + \overline{U_n}\frac{\partial}{\partial n} + \overline{U_z}\frac{\partial}{\partial z}\right](k) \Big\} C$$

$$+\left[-\frac{1}{h}\overline{u_s'^2}\left(\frac{\partial \overline{U_s}}{\partial s} + \frac{\overline{U_n}}{R}\right) - \overline{u_n'^2}\frac{\partial \overline{U_n}}{\partial n}\right] - \overline{u_s'u_n'}\left(\frac{\partial \overline{U_s}}{\partial n} + \frac{1}{h}\frac{\partial \overline{U_n}}{\partial s}\right) + \underline{\underline{\frac{1}{h}\overline{u_s'u_n'}\frac{\overline{U_s}}{R}}} - \left(\overline{u_s'u_z'}\frac{\partial \overline{U_s}}{\partial z} + \overline{u_n'u_z'}\frac{\partial \overline{U_n}}{\partial z}\right) - \left(\frac{1}{h}\overline{u_s'u_z'}\frac{\partial \overline{U_z}}{\partial s} + \overline{u_n'u_z'}\frac{\partial \overline{U_z}}{\partial n} + \overline{u_z'^2}\frac{\partial \overline{U_z}}{\partial z}\right) \Big\} P$$

$$-\frac{1}{h}\frac{\partial}{\partial s}\left(\overline{u_s'\frac{u_i'u_i'}{2}}\right) - \frac{1}{h}\frac{\partial}{\partial n}\left(h\,\overline{u_n'\frac{u_i'u_i'}{2}}\right) - \frac{\partial}{\partial z}\left(\overline{u_z'\frac{u_i'u_i'}{2}}\right) \Big\} T$$

$$+\frac{1}{2}(G + V - \varepsilon)$$

Here, $h = 1 + n/R$, R is the local radius of curvature, and the terms in the last line represent velocity-pressure-gradient correlation (G), viscous diffusion (V), and dissipation rate (ε). The first three lines on the right hand side represent, respectively, advection by phase-averaged flow (C), production rate (P), and turbulent diffusion (T).

The effect of wake curvature on asymmetry in distributions of turbulent stresses has been attributed to the underlined "curvature terms" $\overline{u_s'u_n'}(\overline{U_s}/R)$ (Nakayama 1987; Weygandt & Metha 1995). Since the shear stress changes sign across the wake, it increase the turbulent kinetic energy on the inner side of the wake decreases it on the outer side. This term also increases $\overline{u_s'^2}$ and decrease $\overline{u_n'^2}$ on the inner sides and the trends are reversed on the outer/suction side (both not shown here). Figure 4.14a shows the terms contributing to turbulent kinetic energy production rate for a sample plane, s/c=0.21, close to the point of highest curvature in the near wake. As is evident, indeed the curvature term reduces the turbulent kinetic energy on the suction side and increases it on the pressure side. However, its magnitude is only 20% of the term involving the shear stress, especially $-\overline{u_s'u_n'}\cdot\partial\overline{U}_s/\partial n$, much less than values measured by, e.g. Nakayama (1987). The effect of local shear overwhelms the curvature effect, unlike all the previous studies of isolated curved wakes mentioned before. In figure 4.14b we show that the cross-steam location of peak production agrees very well with the location of peak turbulent kinetic energy on the suction side of the wake. Since production rate increases with *s/c* on the suction side (not shown here) as the wake is sheared, the turbulent kinetic energy decays slowly there.

The dominant contributor to turbulent diffusion is cross-stream transport, i.e.

$$-(1/h)\partial(h\,\overline{u_n'u_i'u_i'}/2)/\partial n$$

which is not shown here. The turbulent diffusion term has peaks that oppose the production rate maxima within the wake, i.e. it distributes the turbulence, but also has two additional positive peaks along the perimeter of the wake. The diffusion terms in the evolution equation of turbulent kinetic energy have been modeled as $\nu_T\nabla^2 k$ in numerous studies (Pope 2000), where ν_T is the eddy viscosity. We can measure the eddy viscosity by matching the modeled and measured production rates (Laurence 2002):

$$\nu_T = -(\overline{u_\alpha'^2}\alpha_s + \overline{u_\gamma'^2}\gamma_s + \overline{u_\beta'^2}\beta_s)/2(\alpha_s^2 + \gamma_s^2 + \beta_s^2)$$

where $(\alpha_s, \beta_s, \gamma_s)$ are eigenvalues of the phase-averaged strain rate tensor, and $(\overline{u_\alpha'^2}, \overline{u_\beta'^2}, \overline{u_\gamma'^2})$ are

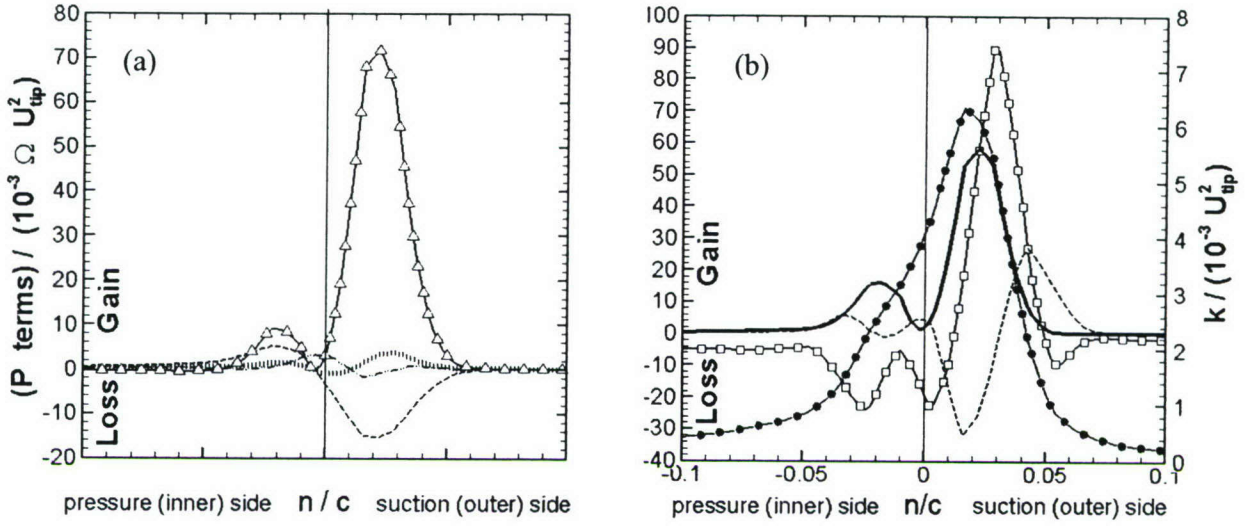

Figure 4.14: (a) Terms contributing to turbulent kinetic energy production at s/c=0.21
(b) Distribution of k and profiles of the terms in the transport equation for k at s/c=0.21.

$\cdots\!-\!\cdot\cdot\cdot -(1/h)\overline{u_s'^2}\left(\partial\overline{U_s}/\partial s+\overline{U_n}/R\right)-\overline{u_n'^2}\partial\overline{U_n}/\partial n$ $\quad -\triangle-\quad -\overline{u_s'u_n'}\left(\partial\overline{U_s}/\partial n+(1/h)\partial\overline{U_n}/\partial s\right)$

$---- +(1/h)\overline{u_s'u_n'}\,\overline{U_s}/R$

$\cdots\cdots\cdots -\left(\overline{u_s'u_z'}\partial\overline{U_s}/\partial z+\overline{u_n'u_z'}\partial\overline{U_n}/\partial z\right)-\left((1/h)\overline{u_s'u_z'}\partial\overline{U_z}/\partial s+\overline{u_n'u_z'}\partial\overline{U_z}/\partial n+\overline{u_z'^2}\partial\overline{U_z}/\partial z\right)$

$-\!\bullet\!- k$; $\quad$ ——— P; $\quad -\!\square\!- C$; $\quad ---- T$.

the corresponding normal Reynolds stress components. Figure 4.15 shows that ν_T varies substantially. Our magnitudes but not necessarily trends, are similar to those obtained by Ha & Lakshminarayana (1982). The eddy viscosity increases with s (not shown), i.e. the turbulent stresses decay at a slower pace compared to the strain. The trends of $\nu_T\nabla^2 k$ agree with the measured values of T in regions of peak production rate (n/c = 0.02 at s/c = 0.21). However, the model under-predicts the peaks of T along the wake perimeter.

Using data obtained in different parts of the flow field, the measured ν_T has been found to be consistently smaller that classical k-ε predictions, i.e. $\nu_T < 0.09k^2/\varepsilon$. The difference is particularly high within sheared wake regions and diminishes far from boundaries and in far wakes. These conclusions are consistent with the comparison between RANS predictions and measured flow discussed in Section 4.3.

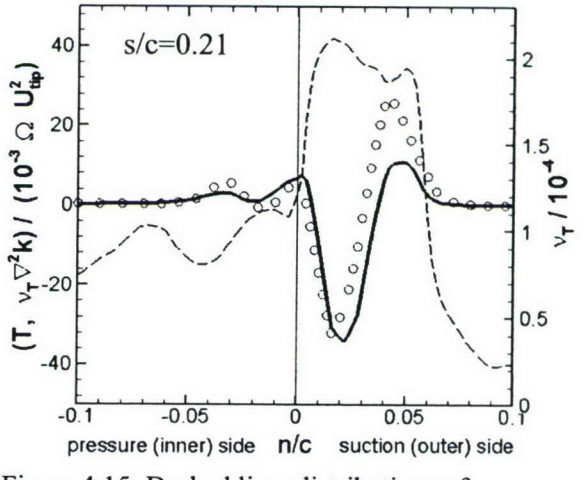

Figure 4.15: Dashed line: distributions of eddy-viscosity; circles: measured turbulent kinetic energy diffusion; solid line: $\nu_T\nabla^2 k$.

4.5 Rotor Boundary Layer Response to an Impinging Wake

Data obtained at different rotor phases (Soranna et al., 2004, 2006c), as the IGV wake is chopped and passes by the rotor blade, also allows us to examine the response of the rotor boundary layer to the mean flow and turbulence introduced by the impinging wake. It should be noted here that typical PIV measurements encounter difficulties near curved solid boundaries due to reflections from the curved wall. Due to the optical index matching, the reflections from walls are minimal in our facility, enabling us to resolve the boundary layers. We focus on the suction side, in regions with adverse pressure gradients, from mid chord to the trailing edge. In this case we have used 2D PIV data. The vorticity and strain rate distribution along with turbulence parameters outside of the rotor boundary layer are used for identifying the approximate boundaries and the center of the impinging IGV wake (see sample in Figure 4.16). Note that in the example shown the distribution is composed from four vector maps, each being an average of 1000 instantaneous distributions.

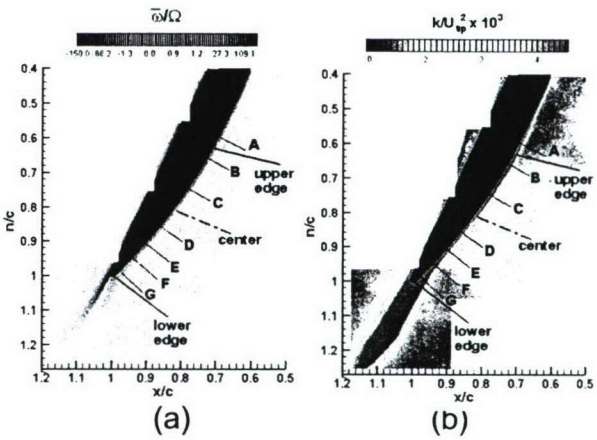

Figure 4.16. (a) Phase-averaged radial vorticity and (b) turbulent kinetic energy as an IGV wake impinges on a boundary layer.

Figure 4.17 compares velocity profiles at the same station, but at different phases for stations D, E, F and G (identified in Figure 4.16). For each velocity profile, the wall-parallel velocity component in the rotor frame of reference, $\overline{U}_s$, is normalized with the local wall parallel relative velocity, $\overline{U}_0$, just outside of the boundary layer, at n/c=3%. As is evident, the structure of the turbulent boundary layer is substantially altered by the interaction with the incident wake. Outside of the wake, the boundary layer grows monotonically and develops an inflection point, which is inherently unstable, as the trailing edge is approached. Within the impinging wake, the boundary layer profiles are thinner and fuller than those located outside of the wake. To determine the causes for these changes, we examine the effect of the impinging wake on the momentum thickness along the suction side. Combining expressions provided in

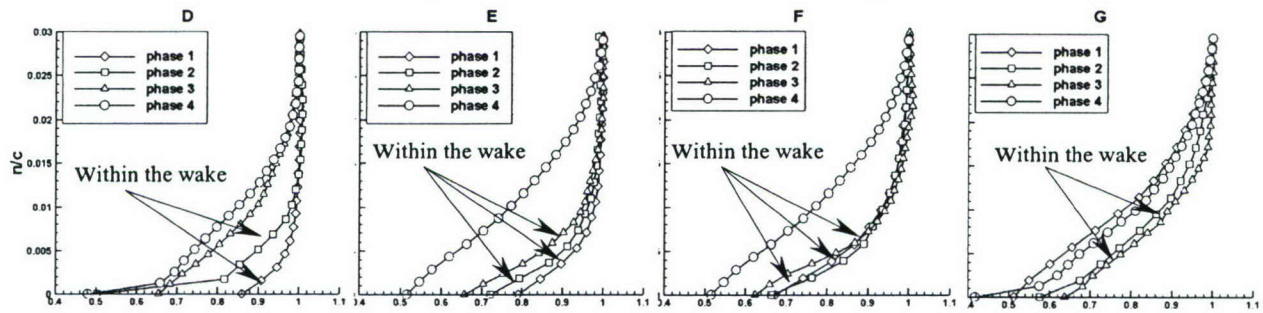

Figure 4.17: Mean boundary layer velocity profiles on the rotor blade at locations D, E, F, and G (see Figure 4.16) at different rotor phases. Profiles measured while the upstream stator wake impinges on the rotor blade at this location are indicated. Velocities are normalized with the local wall parallel relative velocity magnitude measured at a distance n/c=3% from the suction surface.

Lakshminarayana and Govindan (1981) and So and Mellor (1973), assuming a two dimensional motions, but accounting for curvature effects, the evolution equation for the momentum thickness, θ, is

$$\frac{d\theta}{ds} = -\frac{1}{U_{pw}^2}\frac{\partial}{\partial t}\int_0^\infty \left(U_p - \bar{U}_s\right)dn - \left(H+2\right)\frac{\theta}{U_{pw}}\frac{dU_{pw}}{ds} + \frac{u_\tau^2}{U_{pw}^2} - \frac{2}{U_{pw}^2}\int_0^\infty \Omega_n \bar{U}_r dn + q\frac{d\kappa}{ds}$$

$$\delta^* \equiv \int_0^\infty \left(1-\frac{\bar{U}_s}{U_p}\right)dn, \quad \theta \equiv \int_0^\infty \frac{\bar{U}_s}{U_p}\left(1-\frac{\bar{U}_s}{U_p}\right)dn, \quad H \equiv \frac{\delta^*}{\theta}, \quad q = \int_0^\infty n\left(1-\frac{\bar{U}_s}{U_p}\right)dn + 2\int_0^\infty n\frac{\bar{U}_s}{U_p}\left(1-\frac{\bar{U}_s}{U_p}\right)dn$$

Here, $\kappa = 1/R$ is the blade surface curvature, u_τ^2 is the friction velocity, and Ω_n is the wall-normal components of angular velocity of the turbomachine. U_p is the "potential velocity", assumed to be equal to the wall-parallel velocity out side of the boundary layer. Near the wall $U_p = U_{pw}e^{-\kappa n} \approx U_{pw}(1-\kappa n)$, where U_{pw} is the potential velocity at the blade surface, i.e. the velocity that would exist near the blade in the absence of a boundary layer. These trends are supported by the data for regions located outside of the boundary layer (Soranna et al., 2006c). Sample distributions of the dominant terms in the mementuum thickness equation, covering $0.72<s/c<0.93$, are presented in Figure 4.18. The values of $d\theta/ds$ have the highest (negative) magnitude at station 2, i.e. the boundary layer is thinning, close to the upper edge of the wake, and become positive in the forward part of the wake. Behind (above) the wake $d\theta/ds$ is nearly zero in the present phase, but it becomes positive in other phases (not shown). The question is which term causes this effect? The term containing $d\kappa/dx$, i.e. the streamwise variations in curvature, is negligible for the present geometry. The wall shear stress term is small and always positive, i.e. it cannot reduce the boundary layer thickness. To estimate it, we use the Reynolds shear stress within the boundary layer, at about 0.002c from the wall (the closest we can reach with the present data – will be improved in the proposed study).

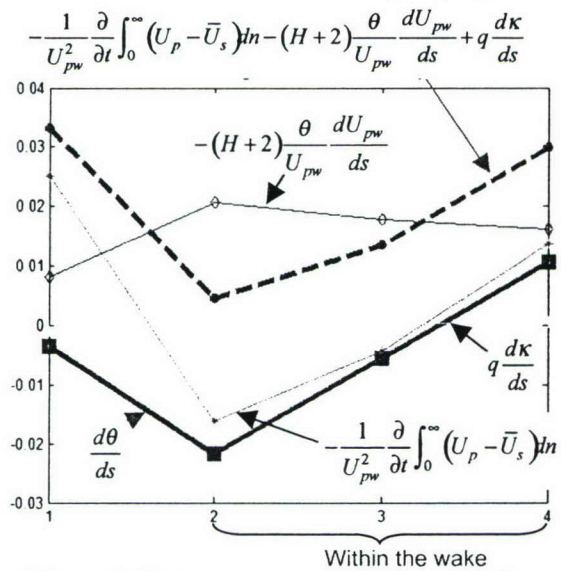

Figure 4.18: Measured terms in the evolution equation for the momentum thickness on the rotor boundary layer in the region impinged by a stator wake.

The convective (second) term on the right hand side of Equation 15 is substantial and positive, i.e. it can only cause streamwise increase θ. The unsteady term (first), obtained from data recorded at 0.1 ms before and after the phase shown here, is positive outside of the wake and negative within it. Thus, of the terms presented here, it is the only one that can reduce the boundary layer thickness within the region covered by the impinging wake. Outside of the wake, the unsteady term is also positive. When all the available contributors are combined, we obtain a distribution that has consistently higher values than $d\theta/ds$. However, the shape of the curve showing the combined terms appears to be quite similar to that of $d\theta/ds$,

but it is shifted upward. We cannot explain the discrepancy between $d\theta/ds$ and the right hand side of Equation 15 using the present data. The Coriolis term, determined from stereo PIV data near the trailing edge that has a lower spatial resolution (§4.4), is only about 12% of unsteady term in station 2, i.e. it cannot explain the discrepancy, but would reduce it. Another ignored effect, which is associated with curvature, is the term $1+n/r$ that should appear in the denominator of the convective term. Adding it term would reduce the convective term by 10%, again in the correct direction, but it will still not be enough to cover the discrepancy. What's missing in the present analysis is the effect of out-of-pane terms, i.e. the terms involving the radial velocity components, as well as derivatives in the r direction (Lakshminarayana and Govindan, 1981)

$$\frac{2}{U_{pe}}\frac{\partial U_{pe}}{\partial r}\int_0^{\delta}\frac{\bar{U}_r}{U_{pe}}dn-\frac{1}{U_{pe}}\frac{\partial U_{pe}}{\partial r}\int_0^{\delta}\frac{\bar{U}_r}{U_{pe}}dn$$

where U_{pe} is the potential flow velocity outside of the boundary layer, and $\bar{U}_r$ is the phase averaged radial velocity. We cannot measure these terms using planar data, and the stereo-PIV data available to us, even in close spaced planes, is not detailed enough to resolve the boundary layer. Such measurements are will be performed as part of the proposed extension to this project. However, these data do indicate that the radial velocity component outside of the boundary layer is negative (which we account for in evaluating the Coriolis term effect), and its magnitude is about 15% of U_{pe}. Thus, its impact on the momentum balance cannot be ignored.

The presently observed trends have far reaching implications as far as predictions of unsteady phenomena in turbomachines. Note that since the boundary layer profile is stabilized by the unsteady contribution, its effect will not be recognized by any steady flow calculation. Only unsteady RANS or LES can potentially resolve this effect. A steady calculation will over-predict the adverse pressure gradient near the trailing edge, maybe even leading to prediction flow separation that is prevented by flow unsteadiness.

4.6 LES Issues: Turbulence Production, and Sub-Grid Scale Energy Flux in The Near Wake

In LES, we solve for the large-scale (resolved) turbulent motions using the spatially filtered Navier Stokes Equations. This filtering process introduces the sub grid scale (SGS) stress tensor, $\tau_{ij}=\widetilde{u_iu_j}-\tilde{u}_i\tilde{u}_j$, where "~" indicates spatial filtering at scale Δ, that must be modeled in terms of resolved flow parameters (Leonard, 1974; Piomelli et al., 1991; Meneveau & Katz, 2000). A key parameter in typical SGS stress models is the so-called SGS dissipation, $\Pi=-\tau_{ij}\widetilde{S}_{ij}$ where $\tilde{S}_{ij}$ is the filtered strain rate tensor. As described in Chow et al. (2005a), the analysis introduced in this section was initiated due to confusion about the relationships between production of turbulent kinetic energy by Reynolds stresses (in RANS sense) and subgrid dissipation (i.e. in LES sense). In the near wake we observed that the latter can be negative (energy backscatter from sub-grid to resolved scales) even when the Reynolds production is positive. A desire to elucidate this paradoxical result has motivated us to develop all the relevant kinetic energy and energy flux terms that result from spatial filtering followed by ensemble averaging of data, as one would do while analyzing LES results. In a highly non-uniform flow field, typical to turbomachines, spatial filtering for LES filters both the fluctuating and mean (phase averaged) flow components.

To avoid confusion, in this section we denote phase averaging by <> and spatial filtering by ~. The total spatially filtered and ensemble averaged kinetic energy, $<\tilde{k}>$, can be decomposed to four parts,

$<\tilde{K}> \equiv 0.5 <\widetilde{u_i u_i}> = K^{mr} + K^{ms} + K^{fr} + K^{fs}$ where

$K^{mr} = 0.5 <\tilde{u}_i><\tilde{u}_i>$ is the mean resolved kinetic energy

$K^{ms} = 0.5(\widetilde{<u_i><u_i>} - <\tilde{u}_i><\tilde{u}_i>)$ is the mean subgrid kinetic energy

$K^{fr} = 0.5 <\tilde{u}_i'\tilde{u}_i'>$ is the fluctuating resolved kinetic energy

$K^{fs} = 0.5(\widetilde{<u_i'u_i'>} - <\tilde{u}_i'\tilde{u}_i'>)$ is the fluctuating subgrid kinetic energy.

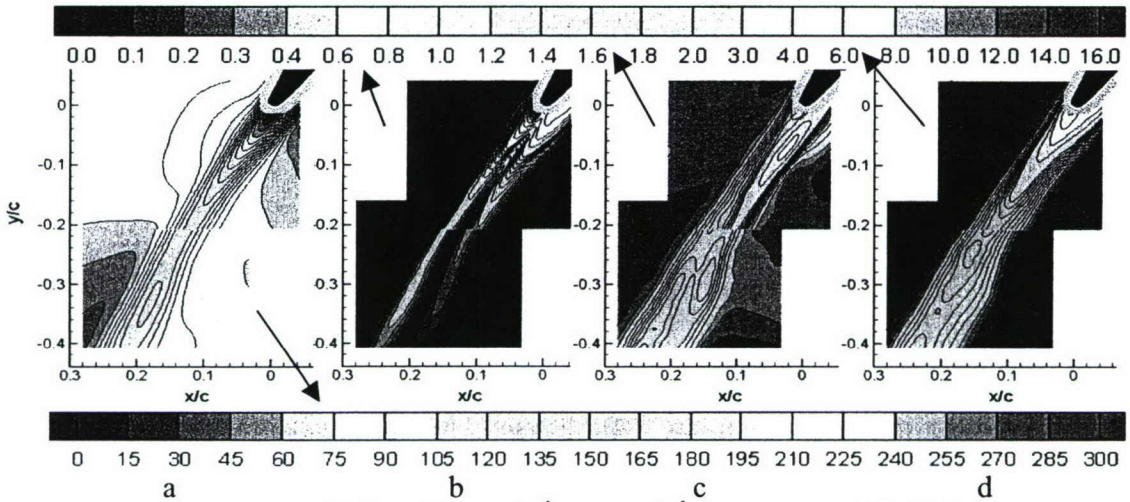

Fig. 4.19: Distributions of a) K^{mr}_{rel}, b) K^{ms}, c) K^{fr}, and d) K^{fs} normalized by $U^2_{tip} \cdot 10^{-3}$. The gray mask around the blade covers points where spatial filtering overlaps with the blade.

Distributions of these components for the rotor near wake, using a box spatial filter of 5x5 vectors (~25% of the near wake width), are presented in Figure 4.19. The values of K^{mr}_{rel}, the only non-Galilean invariant term, are presented in the rotor frame of reference. K^{ms} has a two-layer structure as the boundary layers on both sides of the blade extend to the wake region. It represents the kinetic energy lost when a non-uniform mean flow field is spatially filtered. The distribution of K^{fr}, the resolved part of the turbulent kinetic energy, is biased toward the suction side, indicating higher injections of resolved turbulence from the suction-side boundary layer. The decay of K^{ms} along the wake is faster than that of K^{fr} and K^{fs}. Wake spreading and a fixed filter size contribute to this trend, since the mean-resolved part increases at the expense of the mean-subgrid part. The presence of chopped IGV wake-segments on both sides of the rotor wake is also evident in K^{fr} and K^{fs}.

We have also developed evolution equations for each of the four kinetic energy parts (Chow et al., 2005):

$$\partial K^{mm}/\partial t + < \tilde{u}_j > \partial K^{mm}/\partial x_j = -(-\tau^{m}_{ij} < \tilde{S}_{ij} >) - (-\tau^{f}_{ij} < \tilde{S}_{ij} >) - (R^{r}_{ij} < \tilde{S}_{ij} >) + T^{mm} - \varepsilon^{mm}$$

$$\partial K^{ms}/\partial t + < \tilde{u}_j > \partial K^{ms}/\partial x_j = +(-\tau^{m}_{ij} < \tilde{S}_{ij} >) - (\widetilde{R_{ij} < S_{ij} >} - \widetilde{R_{ij}} < \tilde{S}_{ij} >) + T^{ms} - \varepsilon^{ms}$$

$$\partial K^{fr}/\partial t + < \tilde{u}_j > \partial K^{fr}/\partial x_j = -(- < \tau'_{ij} \tilde{S}'_{ij} >) + (R^{r}_{ij} < \tilde{S}_{ij} >) + T^{fr} - \varepsilon^{fr}$$

$$\partial K^{fs}/\partial t + < \tilde{u}_j > \partial K^{fs}/\partial x_j = +(-\tau^{f}_{ij} < \tilde{S}_{ij} >) + (- < \tau'_{ij} \tilde{S}'_{ij} >) + (\widetilde{R_{ij} < S_{ij} >} - \widetilde{R_{ij}} < \tilde{S}_{ij} >) + T^{fs} - \varepsilon^{fs}_{\nu}$$

where $\tau^{m}_{ij} \equiv \widetilde{< u_i >< u_j >} - < \tilde{u}_i >< \tilde{u}_j >$, $\tau^{f}_{ij} \equiv < \widetilde{u'_i u'_j} > - < \tilde{u}'_i \tilde{u}'_j >$, $\tau'_{ij} = \tau_{ij} - < \tau_{ij} >$, $\tilde{S}'_{ij} = \tilde{S}_{ij} - < \tilde{S}_{ij} >$ and $R^{r}_{ij} \equiv - < \tilde{u}'_i \tilde{u}'_j >$. The energy fluxes between the different kinetic energy parts, denoted as Π (*donor,receiver*), are:

$\Pi(\text{mr,ms}) = -\tau^{m}_{ij} < \tilde{S}_{ij} >$

$\Pi(\text{mr,fs}) = -\tau^{f}_{ij} < \tilde{S}_{ij} >$,

$\Pi(\text{mr,fr}) = R^{r}_{ij} < \tilde{S}_{ij} >$

$\Pi(\text{ms,fs}) = \widetilde{R_{ij} < S_{ij} >} - \widetilde{R_{ij}} < \tilde{S}_{ij} >$

$\Pi(\text{fr,fs}) = - < \tau'_{ij} \tilde{S}'_{ij} >$.

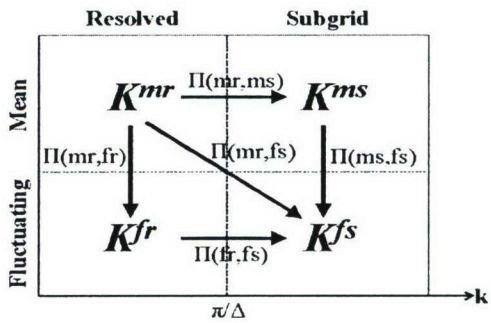

Fig. 4.20: Parts of the kinetic energy, and associated fluxes.

For clarity, they are illustrated in Figure 4.20. The sum of energy fluxes from the resolved to subgrid scales (horizontal direction in Fig. 4.20) is the ensemble averaged SGS energy flux,

$$\Pi = - < \tau_{ij} \tilde{S}_{ij} > = \Pi(\text{mr,ms}) + \Pi(\text{mr,fs}) + \Pi(\text{fr,fs}) .$$

The sum of fluxes from the mean components to the fluctuating parts (downward in Fig. 4.20) is the filtered kinetic energy production rate,

$$\tilde{P} = \widetilde{R_{ij} < S_{ij} >} = \Pi(\text{mr,fr}) + \Pi(\text{mr,fs}) + \Pi(\text{ms,fs})$$

As is evident, Π and $\tilde{P}$ only have one common term, $\Pi(\text{mr,fs})$. The in-plane contributions to the different flux terms are presented in Figure 4.21. Since terms involving the strain tensor require

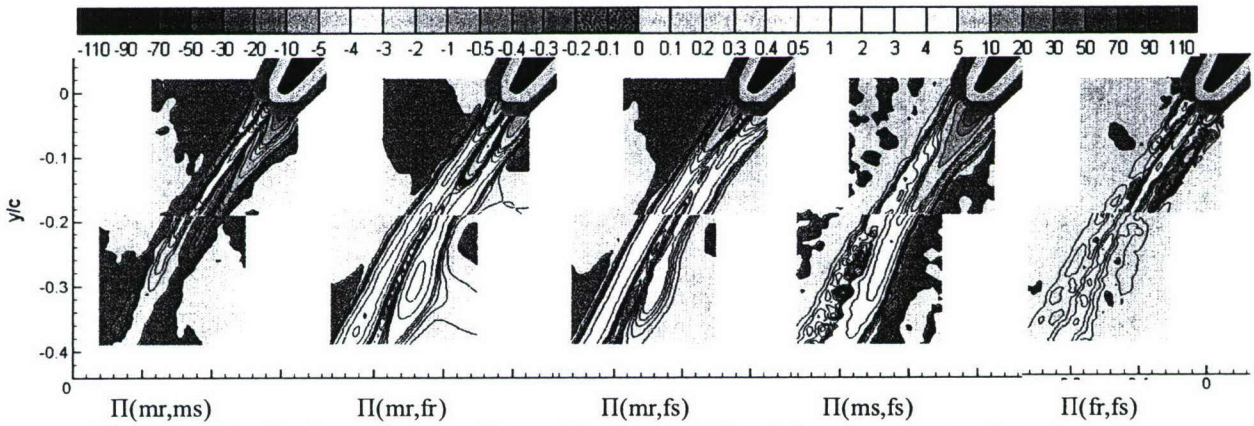

Fig. 4.21: Distributions of energy fluxes. The gray and the pink masks cover points where the spatial filtering and the spatial derivations overlap the blade.

out of plane velocity gradients, even a single plane stereo-PIV data cannot provide all the terms. In studies involving isotropic turbulence one can make various assumptions about relations between in-plane and out-of-plane components (e.g. Liu et al., 1994). However, such assumptions are wrong and lead to absurd conclusions in non-homogeneous an-isotropic turbulence in the rotor passage (we tried). Thus, with single plane PIV data we only have the in-plane part of the energy flux (7/5 of the total flux for isotropic turbulence). In the proposed extension, we will perform simultaneous measurements in two closely spaced planes to obtain the out-of-plane spatial derivatives. One of the benefits will be the correct/full value of SGS dissipation rate.

Also note that $\Pi(mr,ms)$ involves only the mean flow. The negative areas emanating from the boundary layers on both sides of the blade indicate flux from the subgrid to the resolved scales due to the growth of the wake. The highest positive flux occurs from the mean subgrid to the fluctuating subgrid kinetic energies ($\Pi(ms,fs)$). This term dominates the total production rate, i.e. most of the turbulence is produced by the sub-grid mean flow. Negative production of resolved turbulence ($\Pi(mr,fr)$) occurs downstream of the blade trailing edge. These non-equilibrium conditions develop as the boundary layer turbulence is fed into a region with adverse velocity gradients. This analysis highlights why production and SGS dissipation have substantially different trends. Other issues, e.g. role of filter size in comparison to the integral scale of turbulence and methods for calculating spatial derivatives are discussed in Chow et al. (2005a).

4.7 Concluding Comments on our progress

The ability to probe at high resolution any point within the passage is also unique. The data enable us to identify and address fundamental issues in modeling of flow and turbulence that are unique to this highly strained, inhomogeneous, non-equilibrium flow environment.

The sample results provided here do not cover all the complex blade-wake and wake-wake interactions in multistage turbomachines that we have already examined. However, they are sufficient for demonstrating the unique insight that the present data provide, e.g. the ability to measure the variations in boundary layer characteristics on a rotating blade within a multi-blade turbomachine is unique to our optical index-matched facility. Information on other topics can be found in recently published papers. In Chow et al., (2005a) and Soranna et al. (2006b) we introduce a method to scale the mean flow (velocity deficit) profile of the wake, and show that the evolution of turbulence parameters is slower than that of the mean flow. When the wake is sheared, finding scaling parameters for turbulence becomes impossible. Another major topic involving the turbomachinery facility that is not discussed here involves analysis of deterministic stresses and deterministic energy fluxes (Uzol et al., 2002b, 2003a, Meneveau and Katz, 2002). We have also limited most of the present discussion/examples to the mid span region, since trends are simpler to explain there. In Soranna et al. (2007a), we examine flow and turbulence in the tip region at the same level of detail as the mid-span data. The need for full 3D data has been strikingly evident in this region. The hub region with the complexity involving wing-body junctions and transition between rotating to stationary regions also requires attention.

5. Associated Publications Citing AFOSR Support

5.1 Journal Publications

1. Uzol, O., Chow, Y.C., Katz, J., Meneveau, C., (2002), "Unobstructed PIV measurements within an axial turbo-pump using liquid and blades with matched refractive indices," Experiments in Fluids, Vol. 33, pp. 909-919.
2. Meneveau, C., Katz, J., (2002), "A Deterministic Stress Model for Rotor-Stator Interactions in Simulations of Passage-Averaged Flow." Journal of Fluids Engineering, Vol. 124, No. 2, pp. 550-554.
3. Uzol, O., Chow, Y.C., Katz, J., Meneveau, C., (2002), Experimental Investigation of Unsteady Flow Field Within a Two Stage Axial Turbomachine Using Particle Image Velocimetry, J. of Turbomachinery, Vol. 124, pp. 542-552.
4. Chow, Y.C., Uzol, O., Katz, J., (2002), "Flow Non-Uniformities and Turbulent "Hot Spots" Due To Wake-Blade And Wake-Wake Interactions in a Multistage Turbomachine," J. of Turbomachinery, Vol. 124, pp. 553-563.
5. Uzol, O., Chow, Y.C., Katz, J., Meneveau, C., (2003), "Average Passage Flow Field and Deterministic Stresses in The Tip and Hub Regions of A Multi-Stage Turbomachine," J. of Turbomachinery, Vol. 125, pp. 714-725.
6. Chow, Y., Uzol, O., Katz, J., Meneveau, C., (2005), "Decomposition of the Spatially Filtered and Ensemble Averaged Kinetic Energy, the Associated Fluxes and Scaling Trends in a Rotor Wake," Physics of Fluids, Vol. 17, No. 085102.
7. Soranna, F., Chow, Y.C., Uzol, O., Katz, J., (2006) "On The Effect Of IGV Wake Impingement on The Flow Around The Leading Edge of A Rotor Blade," Journal of Turbomachinery, Vol., 128, pp. 82-95.
8. Uzol, O., Brzozowski, D., Chow, Y.C., Katz, J., Meneveau, C., (2007), "A Database of PIV Measurements Within a Turbomachinery Stage and Sample Comparisons With Unsteady RANS," accepted for publication in Journal of Turbulence, DOI: 10.1080/14685240601142867.
9. Soranna, F., Chow, Y.C., Uzol, O., Katz, J., (2007), "Structure of Turbulence Within a Sheared Near Wake of a Turbomachine Rotor Blade," submitted for publication in AIAA Journal.

5.2 Conference papers

1. Uzol, O., Chow, Y.C., Katz, J., Meneveau, C., (2001), "Unobstructed PIV Measurements Within an Axial Turbo-Pump Using Liquid And Blades With Matched Refractive Indices," 4th International Symposium on Particle Image Velocimetry, Göttingen, Germany, September 17-19.
2. Chow, Y.C., Uzol, O., Katz, J., Meneveau, C., (2002), "An Investigation of Axial Turbomachinery Flows Using PIV in an Optically-Unobstructed Facility," The 9th of International Symposium on Transport Phenomena and Dynamics of Rotating Machinery, Honolulu, Hawaii, February 10-14.

3. Uzol, O., Chow, Y.C., Katz, J., Meneveau, C., (2002), Experimental Investigation of Unsteady Flow Field Within a Two Stage Axial Turbomachine Using Particle Image Velocimetry, International Gas Turbine Institute, ASME TURBO EXPO 2002, paper no. GT-2002-30664, Amsterdam, The Netherlands.

4. Chow, Y.C., Uzol, O., Katz, J., (2002), "Flow Non-Uniformities and Turbulent "Hot Spots" Due To Wake-Blade And Wake-Wake Interactions in a Multistage Turbomachine," International Gas Turbine Institute, ASME TURBO EXPO 2002, paper no. GT-2002-30667, Amsterdam, The Netherlands.

5. Uzol, O., Chow, Y.C., Katz, J., Meneveau, C., (2003), "Average Passage Flow Field and Deterministic Stresses in The Tip and Hub Regions of A Multi-Stage Turbomachine," International Gas Turbine Institute, ASME TURBO EXPO 2003, paper no. GT-2003-38598, June 16-19, Atlanta GA.

6. Chow, Y.C., Uzol, O., Katz, J., (2003), "On the Flow and Turbulence Within the Wake and Boundary Layer of A Rotor Blade Located Downstream of an IGV," International Gas Turbine Institute, ASME TURBO EXPO 2003, paper no. GT-2003-38599, June 16-19, Atlanta GA.

7. Chow, Y.C., Uzol, O., Katz, J., Meneveau, C., (2003), "Experimental Study of The Structure of a Rotor Wake in a Complex Turbomachinery Flow," 4TH ASME_JSME Joint Fluids Engineering Conference, Honolulu, Hawaii, USA, July 6-11 (Proceedings of FEDSM-2003), paper No. FEDSM-2003-45575.

8. Soranna, F., Chow, Y.C., Uzol, O., Katz, J., (2004), "Rotor boundary layer response to an impinging wake," paper No. HT-FED2004-56125, Proceedings of HT/FED'04, 2004 Heat Transfer/Fluids Engineering Summer Conference, July 11-15, Charlotte, North Carolina.

9. Uzol, O., Chow, Y.C., Soranna, F., Katz, J., Meneveau, C., (2004), "3-D Measurements of Deterministic Stresses within a Rotor-stator Gap at Mid Span and Tip Regions," paper No. HT-FED2004-56513, Proceedings of HT/FED'04, 2004 Heat Transfer/Fluids Engineering Summer Conference, July 11-15, Charlotte, North Carolina.

10. Uzol, O., Chow, Y.C., Soranna, F., Katz, J., (2004), "3D Structure of a Rotor Wake at Mid-span and Tip Regions," Paper No. AIAA-2004-2552, 34th AIAA Fluid Dynamics Conference and Exhibit, Portland, Oregon, June 28 - July 1.

11. Soranna, F., Chow, Y.C., Uzol, O., Katz, J., (2005) "On The Effect Of IGV Wake Impingement on The Flow Around The Leading Edge of A Rotor Blade," Paper No., GT2005-68801, Proceedings Of ASME, Turbo Expo 2005, June 6-9, 2005, Reno-Tahoe, Nevada, USA.

12. Chow, Y., Uzol, O., Katz, J., Meneveau, C., (2005), "On the Energy Flux between Large, Small, Mean and Fluctuating Parts of the Flow in a Turbomachinery Rotor Wake," Paper No. AIAA 2005-1271, 43rd AIAA Aerospace Sciences Meeting and Exhibit, 10 - 13 Jan., Reno, NV.

13. Brzozowski, D., Uzol, O., Chow, Y.C., Katz, J., Meneveau, M., (2005), "A Comparison of Unsteady RANS Simulations With PIV Data in an Axial Turbomachine," Paper No. FEDSM2005-77318, Proceedings of FEDSM 2005, ASME Fluids Engineering Division Summer Meeting, June 19-23, Houston, TX.

14. Soranna, F., Chow, Y.C., Uzol, O., Katz, J., (2005), "3D Measurements of The Mean Velocity and Turbulence Structure Within The Near Wake of a Rotor Blade," Paper No. FEDSM2005-77315, Proceedings of FEDSM 2005, ASME Fluids Engineering Division Summer Meeting, June 19-23, Houston, TX.

15. Uzol, O., Chow, Y.C., Soranna, F., Katz, J., Meneveau, C., (2005), "Two-Dimensional and Stereoscopic Particle Image Velocimetry Measurements Within an Axial Turbomachine," 3 rd Ankara International Aerospace Conference, Aug. 22-25, Middle East Technical University (METU), Ankara, Turkey.

16. Soranna, F., Chow, Y.C., Uzol, O., Katz, J., (2006), "The Effect of IGV Wake Impingement on a Rotor Boundary Layer," Paper No. AIAA 2006-1305, 44th AIAA Aerospace Sciences Meeting and Exhibit, Jan 9 – 12, Reno, Nevada.

17. Soranna, F., Chow, Y.C., Uzol, O., Katz, J., (2006), "Structure of Turbulence Within a Sheared Wake of a Rotor Blade," Paper No. FEDSM2006-98401, Proceedings of the ASME, Fluids Engineering Division Summer Meeting, Joint U.S. - European Fluids Engineering Summer Meeting, July 17-20, Miami, FL.

18. Soranna, F., Chow, Y.C., Uzol, O., Katz, J., (2006), Evolution of Flow Structure and Turbulence around a Rotor Blade due to Interaction with the Non-Uniform Strain Field Generated by Upstream Blades," 26th Symposium on Naval Hydrodynamics, September 17-22, Rome, Italy.

19. Soranna, F., Chow, Y.C., Uzol, O., Katz, J., (2007), "Flow Structure and Turbulence in the Tip Region of a Multistage Turbomachine Rotor Blade," Paper # GT2007-27590, Accepted for ASME Turbo Expo 2007: Gas Turbine Technical Congress & Exposition, May 14-17, Palais des Congres, Montreal, Canada.

20. Soranna, F., Chow, Y.C., Uzol, O., Katz, J., (2007), "Structure of Turbulence Around The Trailing Edge of a Rotor Blade," Paper No. FEDSM2007-37573, Proceedings Of FEDSM2007, Joint ASME/JSME Fluids Engineering Conference, July 30-August 2, San Diego, CA.

6. Cited References

Adamczyk J.J., Mulac R.A., Celestina M.L., 1986, "A Model for Closing the Inviscid Form of the Average-Passage Equation System," ASME Paper No. 86-GT-227.

Adamczyk J.J.; Celestina M.L.; Beach T.A.; Barnett M., 1990, "Simulation Of Three Dimensional Viscous Flow Within A Multistage Turbine," *J. of Turbomachinery*, **112**, 370

Adamczyk, J. J., 1985, "Model Equation for Simulating Flows in Multistage Turbomachinery," ASME Paper No. 85-GT-226.

Balzani N., Scarano F., Riethmuller M. L., Breugelmans F. A. E., 2000, "Experimental Investigation of the Blade-to-Blade Flow in a Compressor Rotor by Digital Particle Image Velocimetry," *J. of Turbomachinery*, **122**, 743-750.

Batchelor, G.K., Proudman, I., 1954, "The effect of rapid distortion on a fluid in turbulent motion," *Quart. J. Mech. Appl. Maths.* **7**, 83-103.

Bradshaw, P., 1973, "Effects of streamline curvature on turbulent flow," AGARD*ograph* 169.

Brzozowski, D., Uzol, O., Chow, Y.C., Katz, J., Meneveau, M., 2005, "A Comparison of Unsteady RANS Simulations With PIV Data in an Axial Turbomachine," Paper No. FEDSM2005-77318, *ASME Fluids Engineering Division Summer Meeting*, June 19-23, Houston, TX.

Busby J.; Sondak D.; Staubach B.; Davis R., 2000, "Deterministic Stress Modeling of a Hot Gas Segregation in a Turbine," *J. of Turbomachinery*, **122**, 62.

Cerutti S. and C. Meneveau 1998, "Intermittency and relative scaling of subgrid scale energy dissipation in isotropic turbulence", *Phys. Fluids*, **10**, 928-937.

Chen J., C. Meneveau, Katz, J., 2006, "Scale Interactions of Turbulence Subjected to a Straining-Relaxation-Destraining Cycle", *J. Fluid Mech.*, Vol. 562, pp. 123-150.

Chen, J., Katz, J., 2005b, "Elimination of Peak-locking Error in PIV Analysis Using the Correlation Mapping Method," *Measurement Science and Technology*, **16**, 1605-1618.

Chen, J., Katz, J., Meneveau, C., 2005, "The Implication of Mismatch between Stress and Strain-Rate in Turbulence Subjected to Rapid Straining and Destraining on Dynamic LES Models," *J. Fluids Eng.*, **127**, 840-850.

Chow, Y., Uzol, O., Katz, J., Meneveau, C., 2005a, "Decomposition of the Spatially Filtered and Ensemble Averaged Kinetic Energy, the Associated Fluxes and Scaling Trends in a Rotor Wake," *Physics of Fluids*, **17**, No. 085102.

Chow, Y., Uzol, O., Katz, J., Meneveau, C., 2005b, "On the Energy Flux between Large, Small, Mean and Fluctuating Parts of the Flow in a Turbomachinery Rotor Wake," Paper No. AIAA 2005-1271, *43rd AIAA Aerospace Sciences Meeting*, 10 - 13 Jan., Reno, NV.

Chow, Y.C., Uzol, O., Katz, J., 2002a, "Flow Non-Uniformities and Turbulent "Hot Spots" Due To Wake-Blade And Wake-Wake Interactions in a Multistage Turbomachine," *J. of Turbomachinery*, **124**, 553-563.

Chow, Y.C., Uzol, O., Katz, J., 2002b, "Flow Non-Uniformities and Turbulent "Hot Spots" Due To Wake-Blade And Wake-Wake Interactions in a Multistage Turbomachine," *ASME TURBO EXPO*, paper no. GT-2002-30667, Amsterdam, The Netherlands.

Chow, Y.C., Uzol, O., Katz, J., 2003a, "On the Flow and Turbulence Within the Wake and Boundary Layer of A Rotor Blade Located Downstream of an IGV," *ASME TURBO EXPO*, paper no. GT-2003-38599, June 16-19, Atlanta GA.

Chow, Y.C., Uzol, O., Katz, J., Meneveau, C., 2002c, "An Investigation of Axial Turbomachinery Flows Using PIV in an Optically-Unobstructed Facility," *The 9th of International Symposium on Transport Phenomena and Dynamics of Rotating Machinery*, Honolulu, Hawaii, February 10-14.

Chow, Y.C., Uzol, O., Katz, J., Meneveau, C., 2003b, "Experimental Study of The Structure of a Rotor Wake in a Complex Turbomachinery Flow," paper No. FEDSM-2003-45575, *4TH ASME_JSME Joint Fluids Engineering Conference*, Honolulu, Hawaii, July 6-11.

Christensen, K.T., Adrian, R.J., 2002, "Measurement of Instantaneous Eulerian Acceleration Fields by Particle-Image Velocimetry: Method and Accuracy," *Exp. Fluids*, **33**, 759-769.

Day, I. J., 1992, "Stall and surge in Axial Flow Compressors," *VKI Lecture Series, 1992-02.*

De La Riva, D.H., Devenport, W.J., Chittiappa, M., Glegg, S.A.L., 2004, "Behavior of Turbulence Flowing Through a Compressor Cascade," *AIAA J.*, **42,** 1302-1313.

Demuren, A.O., M.M. Rogers, P.A. Durbin, Lele, S.K., 1996, "On Modeling Pressure Diffusion in Non-Homogeneous Flows", in "*Proc. Summer School Progr. 1996*", CTR, Stanford University.

Dong, P., Hsu, T.Y., Atsavapranee P., Wei, T., 2001, "Digital particle image accelerometry," *Exp. Fluids*, **30**, 626-632.

Durbin, P. A., 1996, "On the k-e Stagnation Point Anomaly," *Int. J. Heat and Fluid Flow*, **17**, 89-90.

Durbin, P.A. Speziale, C.G., 1994, "Realizability of Second-Order Closure Via Stochastic Analysis" *J. Fluid Mech.*, **280**, 395-407.

Ganapathisubramani, B., Longmire, E.K., Marusic, I., Pothos, S., 2005, "Dual-Plane PIV Technique to Resolve Complete Velocity Gradient Tensor in a Turbulent Boundary Layer," *Exp. Fluids*, **39**, 222-231.

Germano, M., Piomelli, U., Moin P., Cabot, W., 1991, "A Dynamic Subgrid-Scale Eddy Viscosity Model," *Phys. Fluids A*, **3**, 1760-1765.

Ghosal S., T.S. Lund, P. Moin and K. Akselvoll, 1995, "A Dynamic Localization Model for LES of Turbulenct Flows", *J. Fluid Mech.*, **286**, 229-255.

Gogineni, S. Goss, L., Copenhaver, W., Gorrell, S., 1997, "Development of Digital Two-Color PIV for turbomachinery applications," AIAA Paper No. 97-0494.

Hah, C., Lakshminarayana, B., 1982, "Measurements and prediction of mean velocity and turbulence structure in the near wake of an airfoil," *J. Fluid Mech.*, **115**, 251-282.

Hanjalic K. Launder, B.D., 1972, "A Reynolds Stress Model of Turbulence and its Applications to Thin Shear Flows", *J. Fluid Mech.*, **52**, 609-638.

He, L., Chen, T., Wells, R. G., Li, Y. S., Ning, W., 2002, "Analysis of Rotor-Rotor and Stator-Stator Interferences in Multi-Stage Turbomachines," *Journal of Turbomachinery,* **124**, pp. 564-571.

Hunt, J.C.R., Graham, J.M.R., 1978, "Free-Stream Turbulence Near Plane Boundaries," *J. Fluid Mech.*, **84**, 209-235.

Jakobsen ML, Dewhirst TP, Greated CA, 1997, "Particle Image Velocimetry for Predictions of Acceleration Fields and Force within Fluid Flows," *Meas. Sci. & Technol.*, **8**, 1502-1516.

Jensen, A., Pedersen, G.K., 2004, "Optimization of Acceleration Measurements Using PIV," *Meas. Sci. Technol.*, **15**, 2275-2283.

Jensen, A., Pedersen, G.K., Wood, D.J., 2003, "An Experimental Study of Wave Run-Up at a Steep Beach," *J. Fluid Mech.*, **486**, 161-188.

John, J., Schobeiri M.T., 1996, Development of a Two-Dimensional Turbulent Wake in a Curved Channel with a Positive Streamwise Pressure Gradient. *J. Fluids Eng.*. **118**, 292-299.

Jones W.P. and P. Musonge, 1988, "Closure of The Reynolds Stress and Scalar Flux Equations". *Phys. Fluids*, **31**, 3589-3604.

Koyama, H. 1983 Effects of Streamline Curvature on Laminar and Turbulent Wakes. In *Proc.* of *Fourth Symp. on Turbulent Shear Flows, Karlsruhe, Germany*, 6.32-6.37.

La Porta, A., Voth, G.A., Crawford, A.M., Alexander, J., Bodenschatz, E., 2001, "Fluid particle accelerations in fully developed turbulence," *Nature*, **409**, 1017-1019.

Lakshminarayana, B., 1996, *Fluid dynamics and heat transfer of turbomachinery.* John Wiley & Sons.

Lakshminarayana, B., and Govindan, T. R., 1981, "Analysis of Turbulent Boundary Layer on Cascade and Rotor Blades of Turbomachinery," *AIAA Journal*, **19**, 1333-1341.

Lauder B.E., Reece, G.J. and W. Rodi , 1975, "Progress in the Development of a Reynolds-Stress Turbulence Closure", *J. Fluid Mech.*, **68**, 537-566.

Launder, B. E. (1989), "Second-Moment Closure and Its Use in Modeling Turbulent Industrial Flows," *Int. J. Numerical Meth. Fluids,* **9**, 963-985.

Laurence D., 2002, "Applications of Reynolds averaged Navier Stokes equations to industrial flows," *Von Karman Inst. Lect. Series: Introduction to turbulence modeling.*

Lee, M.J. & Reynolds W.C., 1985, "Numerical experiments on the structure of homogeneous turbulence," *Technical Report TF-24*, Stanford University.

Lejambre C.R., Zacharias R.M., Biederman B.P., Gleixner A.J., Yetka C.J., 1998, "Development And Application Of A Multistage Navier-Stokes Solver. Part II: Application To A High Pressure Compressor Design," *J. Turbomachinery*, **120**, 215.

Leonard, A., 1974, "Energy Cascade in Large-Eddy Simulations of Turbulent Fluid Flows," *Adv. Geophys*, **18**, 237.

Lien, F. S., Leschziner, M.A., 1994, "Assessment of Turbulent Transport Models Including Non-Linear RNG Eddy-Viscosity Formulation and Second-Moment Closure for Flow over a Backward-Facing Step," *Computers & Fluids*, **23**, 983-1004.

Lilly, D.K., 1992, "A Proposed Modification of the Germano-Subgrid-Scale Closure Method," *Physics of Fluids A-Fluid Dynamics*, **4**, 633-635.

Liu, S., Katz, J., Meneveau, C., 1999, "Evolution and Modeling of Subgrid Scales During Rapid Straining of turbulence", *J. Fluid Mech.*, **387**, 281–320.

Liu, S., Meneveau, C., Katz, J., 1994, "On the Properties of Similarity Subgrid-Scale Models as Deduced from Measurements in a Turbulent Jet," *J. Fluid Mech.*, **275**, 83-119.

Liu, S., Meneveau, C., Katz, J., 1995, "Experimental Study of Similarity Subgrid-Scales Models of Turbulence in The Far Field of a Jet", *J. Applied Scientific Research*, **54**, 177-190.

Liu, X., Katz, J., 2005, "Instantaneous Pressure and Material Acceleration Measurements using a Four Exposure PIV System," *6th Int. Symp. on Particle Image Velocimetry*, Pasadena, CA, September 21-23.

Liu, X., Katz, J., 2006, "Instantaneous Pressure and Material Acceleration Measurements using a Four Exposure PIV System," *Exp. in Fluids*, in press.

Lumley J.L., 1975, "Pressure-strain correlation," *Phys. Fluids*, **18**, 750.

Lumley, J.L., 1978, "Computational modeling of turbulent flows," *Advances in Applied Mechanics*, **18**, 123-176.

Meneveau C., Katz J., 2002, "A Deterministic Stress Model for Rotor-Stator Interactions in Simulations of Average-Passage Flow," *J. Fluids Engineering*, **124**, 550-554.

Meneveau, C., Katz, J., 2000, "Scale-Invariance and Turbulence Models for Large-Eddy Simulation," *Annu. Rev. Fluid Mech.*, **32**, pp. 1-32.

Menon, S., P.K. Yeung, Kim, W.W., 1996, "Effect of Subgrid Models on the Computed Interscale Energy Transfer in Isotropic Turbulence," *Comput. Fluids,* **25**, 165-180.

Moin, P., Mahesh, K., 1998, "Direct Numerical Simulation: a tool in turbulence research," *Annu. Rev. Fluid Mech.,* **30**, 539-578.

Nakayama, A., 1987, "Curvature and Pressure-Gradient Effects on a Small-Defect Wake," *J. Fluid Mech.* **175**, 215-246.

Nimmo Smith, W. A. M., Katz, J., Osborn, T. R., 2005, "On the Structure of Turbulence and Dynamics of subgrid-Scale Stresses in the Bottom Boundary Layer of the Coastal Ocean," *J. Physical Oceanography,* **35**, 72-93.

Ott, S., Mann, J., 2000, "An Experimental Investigation of the Relative Diffusion of Particle Pairs in Three-Dimensional Turbulent Flow," *J. Fluid Mech.*, **422**, 207-223.

Pampreen, R.C., 1993, *Compressors Stall and Surge*, Concepts, Library of Congress, Card #. 92-70348.

Perot, B., Moin, P., 1995, "Shear-Free Turbulent Boundary-Layers.1. Physical Insights into Near-Wall Turbulence," *J. Fluid Mech.*, **295**, 199-227.

Piomelli, U., Balaras, E., 2002, "Wall-Layer Models for LES," *Annu Rev. Fluid Mech.*, **34**, 349-374.

Piomelli, U., Cabot, W. H., Moin, P., Lee, S., 1991, "Subgrid-Scale Backscatter in Turbulent and Transitional Flows," *Phys. Fluids A*, **3**, 1766-71.

Piomelli, U., 1999, "Large Eddy Simulation: Achievements and Challenges," *Progress in Aerospace Sciences*, **35**, 335-362.

Pope, S.B., 2000, *Turbulent flows*, Cambridge Univ. Press.

Porté-Agel, F., Meneveau, C., Parlange, M.B., 2000, "A Scale-Dependent Dynamic Model for Large Eddy Simulation: Applications to a Neutral Atmospheric Boundary Layer," *J. Fluid Mech.*, **415**, 261-284.

Prato, J., Lakshminarayana B., Suryavamshi N., 1997, "Exit Flow Field of an Embedded Stator in a Multi-Stage Compressor," *J. of Propulsion and Power*, **13**, 169-177.

Prato, J., Lakshminarayana B., Suryavamshi N., 1998, "Steady and Unsteady Three-Dimensional Flow Field Downstream of an Embedded Stator in a Multi-Stage Axial Flow Compressor Part I: Unsteady Velocity Field," ASME Paper No. 98-GT-521.

Raffel, M., Willert, C., and J. Kompenhans, 1998, *Particle Image Velocimetry*, Springer-Verlag.

Ramjee, V., Neelakandan, D., 1989, "Development of Wake of a Rectangular Cylinder in a Curved Stream," *Exps. Fluids*, **7**, 395-399.

Rhie C.M., Gleixner, A.J., Spear, D.A., Fischberg, C.J., Zacharias, R.M., 1998, "Development and Application of a Multistage Navier-Stokes Solver. Part I: Multistage Modeling Using Body Forces and Deterministic Stresses," *J. Turbomachinery*, **120**, 205.

Roth, G. I., Katz, J., 2001, "Five Techniques for Increasing the Speed and Accuracy of PIV Interrogation," *Meas. Sci. Technol.*, 12, 238-245.

Roth, G. I., Mascenik, D. T., Katz, J., 1999, "Measurements of The Flow Structure and Turbulence Within A Ship Bow Wave," *Phys. Fluids*, **11**, 3512-3523.

Rotta J., 1951, "Statistical Theory for Inhomogeneous Turbulence," *Z. für Physik*, **129**, 257-272, Transl. W. Rodi, Imp. Coll. Rep. TWF/TN/38.

Sanders, A.J., Papalia J., Fleeter S., 2002, "Multi-Blade Row Interactions in a Transonic Axial Compressor: Part I-Stator Particle Image Velocimetry (PIV) Investigation," *J. of Turbomachinery*, **124**, 10-18.

Shih T.H., Lumley, J.L., 1985, "Modeling of Pressure Correlation Terms in Reynolds Stress and Scalar Flux Equations", FDA 85-3, Cornell University.

Sinha, M., Katz, J., 2000, "Quantitative Visualization of the Flow in a Centrifugal Pump With Diffuser Vanes-I: On Flow Structures and Turbulence," *J. Fluids Eng.*, **122**, 97-107.

Sinha, M., Katz, J., and Meneveau, C., 2000, "Quantitative Visualization of the Flow in a Centrifugal Pump With Diffuser Vanes-II: Addressing Passage-Averaged and Large-Eddy Simulation Modeling Issues in Turbomachinery Flows," *J. Fluids Eng.*, **122**, 108-116.

Sinha, M., Pinarbasi, A., Katz, J., 2001, "The Flow Structure During Onset and Developed States of Rotating Stall Within a Vaned Diffuser of a Centrifugal Pump," *J. Fluids Eng.*, **123**, 490-499.

So, R. M. C., Mellor, G. L., 1973, "Experiment on Convex Curvature Effects in Turbulent Boundary Layers," *J. Fluid Mech.*, **60**, 43-62.

So, R.M.C., Mellor, G.L., 1972, "An Experimental Investigation of Turbulent Boundary Layers Along Curved Surfaces," *NASA CR-1940*.

Soranna, F., Chow, Y.C., Uzol, O., Katz, J., 2004, "Rotor Boundary Layer Response To an Impinging Wake," paper No. HT-FED2004-56125, *ASME Heat Transfer/Fluids Engineering Summer Conference*, July 11-15, Charlotte, NC.

Soranna, F., Chow, Y.C., Uzol, O., Katz, J., 2005a, "On The Effect Of IGV Wake Impingement on The Flow Around The Leading Edge of A Rotor Blade," Paper No., GT2005-68801, *ASME, Turbo Expo*, June 6-9, Reno, NV.

Soranna, F., Chow, Y.C., Uzol, O., Katz, J., 2005b, "3D Measurements of The Mean Velocity and Turbulence Structure Within The Near Wake of a Rotor Blade," Paper No. FEDSM2005-77315, *ASME Fluids Engineering Division Summer Meeting*, June 19-23, Houston, TX.

Soranna, F., Chow, Y.C., Uzol, O., Katz, J., 2006a, "On The Effect Of IGV Wake Impingement on The Flow Around The Leading Edge of A Rotor Blade," *J. of Turbomachinery*, **128**, 82-95.

Soranna, F., Chow, Y.C., Uzol, O., Katz, J., 2006b, "Structure Of Turbulence Within a Sheared Near Wake of a Turbomachine Rotor Blade," submitted for publication in AIAA Journal.

Soranna, F., Chow, Y.C., Uzol, O., Katz, J., 2006c, "The Effect of IGV Wake Impingement on a Rotor Boundary Layer," Paper No. AIAA 2006-1305, *44th Aerospace Sciences Mtg.*, Jan 9 – 12, Reno, NV.

Soranna, F., Chow, Y.C., Uzol, O., Katz, J., 2006d, "Structure of Turbulence Within a Sheared Wake of a Rotor Blade," Paper No. FEDSM2006-98401, Joint U.S. - European Fluids Engineering Summer Meeting, July 17-20, Miami, FL.

Soranna, F., Chow, Y.C., Uzol, O., Katz, J., 2006e, Evolution of Flow Structure and Turbulence around a Rotor Blade due to Interaction with the Non-Uniform Strain Field Generated by Upstream Blades," 26th Symposium on Naval Hydrodynamics, September 17-22, Rome, Italy.

Soranna, F., Chow, Y.C., Uzol, O., Katz, J., 2007a, "Flow Structure and Turbulence in the Tip Region of a Multistage Turbomachine Rotor Blade," Paper # GT2007-27590, Accepted for ASME Turbo Expo 2007: Gas Turbine Technical Congress & Exposition, May 14-17, Palais des Congres, Montreal, Canada.

Soranna, F., Chow, Y.C., Uzol, O., Katz, J., 2007b, "Structure of Turbulence Around The Trailing Edge of a Rotor Blade," Paper No. FEDSM2007-37573, Proceedings Of FEDSM2007, Joint ASME/JSME Fluids Engineering Conference, July 30-August 2, San Diego, CA.

Speziale, C.G., S. Sarkar, T.B. Gatski, 1991, "Modelling the pressure-strain correlation of turbulence: and invariant dynamical systems approach", *J. Fluid Mech.* **227**, 245-272.

Sridhar, G., Katz, J., 1995, "Lift and Drag Forces on Microscopic Bubbles Entrained by a Vortex," *Physics Fluids*, **7**, 389-399.

Suryavamshi N., Lakshminarayana B., Prato J., 1998, "Steady and Unsteady Three-Dimensional Flow Field Downstream of an Embedded Stator in a Multi-Stage Axial Flow Compressor Part II: Composite Flow Field," ASME Paper No. 98-GT-522.

Suryavamshi N., Lakshminarayana B., Prato J., 1998, "Steady and Unsteady Three-Dimensional Flow Field Downstream of an Embedded Stator in a Multi-Stage Axial Flow Compressor Part III: Deterministic Stress and Heat Flux Distribution and Average-Passage Equation System," ASME Paper No. 98-GT-523.

Tao, B., Katz, J., Meneveau, C., 2002, "Holographic PIV Measurements of the Structure of SGS Stress Eigenvectors and their alignment Relative to Parameters Based on the Filtered Velocity Gradients," *J. Fluid Mech.*, **457**, 35-78.

Tisserant D., Breugelmans F.A.E., 1997, "Rotor Blde-to-Blade Measurements Using Particle Image Velocimetry," *J. of Turbomachinery*, **119**, 176-181.

Uzkan, T., Reynolds, W.C., 1967, "A Shear-Free Turbulent Boundary Layer," J. Fluid Mech., **28**, 803-821.

Uzol, O., Brzozowski, D., Chow, Y.C., Katz, J., Meneveau, C., 2006, "A Database of PIV Measurements Within a Turbomachinery Stage and Sample Comparisons With Unsteady RANS," Submitted for publication in J. of Turbulence.

Uzol, O., Chow, Y.C., Katz, J., Meneveau, C., 2001, "Unobstructed PIV Measurements Within an Axial Turbo-Pump Using Liquid And Blades With Matched Refractive Indices," *4th International Symposium on Particle Image Velocimetry*, Göttingen, Germany, September 17-19.

Uzol, O., Chow, Y.C., Katz, J., Meneveau, C., 2002a, "Unobstructed PIV measurements within an axial turbo-pump using liquid and blades with matched refractive indices," *Exp. in Fluids*, **33**, 909-919.

Uzol, O., Chow, Y.C., Katz, J., Meneveau, C., 2002b, "Experimental Investigation of Unsteady Flow Field Within a Two Stage Axial Turbomachine Using Particle Image Velocimetry," *J. of Turbomachinery*, **124**, 542-552.

Uzol, O., Chow, Y.C., Katz, J., Meneveau, C., 2002c, "Experimental Investigation of Unsteady Flow Field Within a Two Stage Axial Turbomachine Using Particle Image Velocimetry," *ASME TURBO EXPO*, paper no. GT-2002-30664, Amsterdam, The Netherlands.

Uzol, O., Chow, Y.C., Katz, J., Meneveau, C., 2003a, "Average Passage Flow Field and Deterministic Stresses in The Tip and Hub Regions of A Multi-Stage Turbomachine," *J. of Turbomachinery*, **125**, 714-725.

Uzol, O., Chow, Y.C., Katz, J., Meneveau, C., 2003b, "Average Passage Flow Field and Deterministic Stresses in The Tip and Hub Regions of A Multi-Stage Turbomachine," *ASME TURBO EXPO*, paper no. GT-2003-38598, June 16-19, Atlanta GA.

Uzol, O., Chow, Y.C., Soranna, F., Katz, J., 2004a, "3D Structure of a Rotor Wake at Mid- span and Tip Regions," Paper # AIAA-2004-2552, *34th AIAA Fluid Dyn. Conf.*, Portland, OR, June 28-July 1.

Uzol, O., Chow, Y.C., Soranna, F., Katz, J., Meneveau, C., 2004b, "3-D Measurements of Deterministic Stresses within a Rotor-stator Gap at Mid Span and Tip Regions," paper No. HT-FED2004-56513, *ASME Heat Transfer/Fluids Eng. Summer Conference*, July 11-15, Charlotte, NC.

Uzol, O., Chow, Y.C., Soranna, F., Katz, J., Meneveau, C., 2005, "Two-Dimensional and Stereoscopic Particle Image Velocimetry Measurements Within an Axial Turbomachine," *3 rd Ankara International Aerospace Conference*, Aug. 22-25, Middle East Technical University (METU), Ankara, Turkey.

Uzol, O., Brzozowski, D., Chow, Y.C., Katz, J., Meneveau, C., (2007), "A Database of PIV Measurements Within a Turbomachinery Stage and Sample Comparisons With Unsteady RANS," accepted for publication in Journal of Turbulence, DOI: 10.1080/14685240601142867

Van de Wall A.G., Kadambi J.R., Adamczyk, J.J., 2000, "A Transport Model for the Deterministic Stresses Associated with Turbomachinery Blade Row Interactions," *J. of Turbomachinery*, **122**, 593-603.

van Hout, R., Zhu, W., Luznik, L., Katz, J. Kleissl, J., Parlange, M., 2005, "PIV Measurements in the Atmospheric Boundary Layer Within and Above a Mature Corn Canopy. Part A: Statistics and Small Scale Isotropy," Submitted for publication in Journal of Atmospheric Sciences.

Voth, G.A., Satyanarayan, K., Bodenschatz, E., 1998, "Lagrangian acceleration measurements at large Reynolds numbers," *Phys. Fluids*, **10**, 2268-2280.

Wernet, M. P., 2000, "Development of Digital Particle Imaging Velocimetry for use in Turbomachinery", *Experiments in Fluids*, **28**, 97-115.

Weygandt, J.H., Mehta, R.D., 1995, "Three-Dimensional Structure of Straight and Curved Plane Wakes, *J. Fluid Mech.*, **282**, 279-311.